AGU Advances

RESEARCH ARTICLE
10.1029/2021AV000470

Diverging Fates of the Pacific Ocean Oxygen Minimum Zone and Its Core in a Warming World

Julius J. M. Busecke[1], Laure Resplandy[2], Sam J. Ditkovsky[3], and Jasmin G. John[4,5]

[1]Lamont-Doherty Earth Observatory of Columbia University, New York, NY, USA, [2]Department of Geosciences, High Meadows Environmental Institute, Princeton University, Princeton, NJ, USA, [3]Program in Atmospheric and Oceanic Sciences, Princeton University, Princeton, NJ, USA, [4]NOAA/OAR/Geophysical Fluid Dynamics Laboratory, Princeton, NJ, USA, [5]NOAA/OAR/Atlantic Oceanographic and Meteorological Laboratory, Miami, FL, USA

Key Points:

- The Pacific oxygen minimum zone (OMZ) will expand but its core might contract under sustained anthropogenic forcing
- Non-thermal changes (ocean circulation and biology) dictate the shift from core contraction to OMZ expansion
- The OMZ expansion would compress the habitat of marine species and impact ecosystems and ecosystem services

Supporting Information:

Supporting Information may be found in the online version of this article.

Correspondence to:

J. J. M. Busecke,
julius@ldeo.columbia.edu

Citation:

Busecke, J. J. M., Resplandy, L., Ditkovsky, S. J., & John, J. G. (2022). Diverging fates of the Pacific Ocean oxygen minimum zone and its core in a warming world. *AGU Advances*, *3*, e2021AV000470. https://doi.org/10.1029/2021AV000470

Received 10 MAY 2021
Accepted 13 AUG 2022

Peer Review The peer review history for this article is available as a PDF in the Supporting Information.

Author Contributions:

Conceptualization: Julius J. M. Busecke, Laure Resplandy
Data curation: Jasmin G. John
Formal analysis: Julius J. M. Busecke, Laure Resplandy, Sam J. Ditkovsky
Funding acquisition: Laure Resplandy
Investigation: Julius J. M. Busecke, Laure Resplandy, Sam J. Ditkovsky
Methodology: Julius J. M. Busecke

Abstract Global ocean oxygen loss is projected to persist in the future, but Earth system models (ESMs) have not yet provided a consistent picture of how it will influence the largest oxygen minimum zone (OMZ) in the tropical Pacific. We examine the change in the Pacific OMZ volume in an ensemble of ESMs from the CMIP6 archive, considering a broad range of oxygen (O_2) thresholds relevant to biogeochemical cycles and ecosystems (5–160 μmol/kg). Despite OMZ biases in the historical period of the simulations, the ESM ensemble projections consistently fall into three regimes across ESMs: an expansion of low oxygenated waters (+0.8 [0.6, 1.0] × 10^{16} m^3/century for $O_2 \leq 120$ μmol/kg, ESM median and interquartile range); a slight contraction of the OMZ core although more uncertain across ESMs (−0.1 [−0.5, 0.0] × 10^{16} m^3/century for $O_2 \leq 20$ μmol/kg); and at the transition from contraction to expansion regimes, a spatial redistribution but near-zero change in the volume of hypoxic waters (0.0 [−0.3, +0.1] × 10^{16} m^3/century for $O_2 \leq 60$ μmol/kg). Changes in circulation and biology dictate the shift from expansion to contraction. Specifically, reduced subtropical ventilation controls the expansion of low oxygenated waters, while a combination of circulation and biological changes explains the contraction of the core (likely changes in mixing, reduced intermediate ventilation and oxygen demand). Increased model complexity (e.g., ecosystem dynamics and equatorial circulation) likely stabilize the OMZ response, suggesting that future changes might lie in the lower bound of current projections. The expansion of low oxygenated waters which delimit the optimum habitat of numerous marine species would severely impact ecosystems and ecosystem services.

Plain Language Summary Expansion of ocean areas with low oxygen concentrations threatens marine animals and could increase the production of greenhouse gases that warm the Earth. An essential question is how these low oxygen "blobs," called oxygen minimum zones (OMZs), will evolve in the future. OMZs are difficult to simulate in climate models because they result from two strongly opposing processes: Physical supply of oxygen via the ocean circulation and oxygen consumption by biological respiration. Previous studies using older generations of models could not conclude whether the largest of these zones in the Pacific would grow or shrink in the future. We show that the Pacific OMZ will grow in response to climate change but that its core—where oxygen is lowest—will shrink. This expansion of the broad OMZ is caused by a weaker supply of oxygen rich waters by ocean circulation, whereas the contraction of the OMZ is influenced by a combination of changes in ocean circulation and biological activity. The expansion of the outer OMZ is likely bad news for the marine species that suffer in low oxygen conditions, and the people that depend on them (fishing and tourism).

1. Introduction

The ocean has lost dissolved oxygen (O_2) in response to global warming in the past 50 years (~2% globally, Keeling et al., 2010; Ito et al., 2017; Levin, 2018; Schmidtko et al., 2017). A serious threat of this systematic ocean deoxygenation is the expansion of tropical oxygen minimum zones (OMZs), where low O_2 levels threaten marine life (Vaquer-Sunyer & Duarte, 2008; Stramma et al., 2011; do Rosário Gomes et al., 2014) and perturb the carbon and nitrogen cycles, potentially acting as an amplifying feedback on climate change (Keeling et al., 2010; Levin, 2018; Stramma et al., 2008). Global upper ocean deoxygenation is projected to continue in the 21st century, especially if greenhouse gas emissions are not rapidly curtailed (Bopp et al., 2013; Kwiatkowski et al., 2020). There has been, however, no consensus on how the OMZs will evolve in the future (e.g., Resplandy, 2018).

Software: Julius J. M. Busecke, Sam J. Ditkovsky
Supervision: Laure Resplandy
Visualization: Julius J. M. Busecke, Sam J. Ditkovsky
Writing – original draft: Julius J. M. Busecke, Laure Resplandy, Sam J. Ditkovsky, Jasmin G. John
Writing – review & editing: Julius J. M. Busecke, Laure Resplandy, Sam J. Ditkovsky, Jasmin G. John

The Tropical Pacific Ocean hosts the largest OMZ in the global ocean. It is found in the so-called "shadow zones" of the subsurface ocean (~200 to 2,000 m, Figure 1), characterized by weak ventilation, long water residence time and highly productive surface upwelling systems that boost subsurface O_2 biological demand (Luyten et al., 1983; Paulmier & Ruiz-Pino, 2009; Pedlosky, 1986). The oxygenation of the tropical Pacific Ocean and the shape of the OMZ are set by the advective supply of oxygenated surface waters to the interior, and the biological consumption of O_2 along these advective pathways. The advective O_2 supply is largely sustained by shallow subtropical cells in the thermocline and intermediate sub-thermocline waters (Duteil et al., 2021; Gnanadesikan et al., 2007, 2012; Llanillo et al., 2018; Margolskee et al., 2019; Schott et al., 2004). There are, however, no direct advective pathways into the OMZ interior (Luyten et al., 1983; Pedlosky, 1986). The evolution of the OMZ core is therefore determined by changes in the balance between biological consumption and the slow supply of oxygen by turbulent mixing processes, in particular due to mesoscale dynamics (eddies, tropical instability waves) (Lévy et al., 2021).

Uncertainties in the spatial and temporal evolution of the Pacific OMZ severely restrict our ability to anticipate its ecological, climatic, and societal impacts. Observations suggest that the Pacific OMZ shrunk for most of the 20th century but expanded after 1970 (Cardich et al., 2019; Deutsch et al., 2014; Stramma et al., 2008). Locally, interannual to decadal variability can be high and some studies found a deoxygenation, for example off the coast of Peru (Espinoza-Morriberón et al., 2021). Prior studies showed that Earth system models (ESMs) from the Coupled Model Intercomparison Project Phase 5 (CMIP5; Taylor et al., 2011) and Phase 6 (CMIP6; Eyring et al., 2016) projected disparate trends in oxygen in the subsurface tropical Pacific Ocean during the 21st century, with some models simulating an oxygen loss and others an oxygen gain (Bopp et al., 2013, 2017; Kwiatkowski et al., 2020). Cabré et al. (2015) concluded that these disparities explained the contradicting trends in Pacific OMZ volume in CMIP5 models, with projected volume changes between −15% and +15%. Despite these inconsistencies in the fate of the OMZs, CMIP5 ESMs consistently projected a global O_2 loss in response to ocean warming, which makes O_2 less soluble and limits the transfer of surface waters to the deeper ocean and the ventilation of the ocean interior (Bopp et al., 2017; Cabré et al., 2015). The CMIP5 models also projected a reduction in the O_2 demand in the subsurface, tied to weaker surface biological productivity and particle export to depth (Bopp et al., 2013). Yet, studies concluded that ESMs disagreed on how strongly these circulation and biological changes offset each other in space and time (Bopp et al., 2017) and projected either a contraction or an expansion of the OMZ (Cabré et al., 2015; Frölicher et al., 2020).

The influence of ocean circulation emerged as a particularly important factor in these uncertainties. For instance, ESMs that projected a larger expansion of the OMZ in the equatorial Pacific by the year 2100 were those that simulated a stronger decline in the equatorial Pacific circulation, largely exceeding the biological changes (Shigemitsu et al., 2017). Another factor contributing to the uncertain fate of the OMZs is the O_2 threshold that was chosen to define the OMZs (commonly defined as the volume of ocean with O_2 concentrations below a certain threshold). Thresholds used in the literature differ widely, ranging from suboxic ($O_2 < 5$ μmol/kg) to hypoxic (typically $O_2 < 30$, 50, or 60 μmol/kg) or more losely defined low oxygenated waters (typically $O_2 < 80$ or 100 μmol/kg) (Bopp et al., 2013; Cabré et al., 2015; Cocco et al., 2012). For instance, in the Pacific Ocean, Cabré et al. (2015) showed that 7 out of 9 CMIP5 models projected an expansion of low oxygenated waters ($O_2 < 100$ μmol/kg), but found disparate trends for hypoxic waters ($O_2 < 30$ μmol/kg) with about half of the models projecting a contraction while the other half projected an expansion.

Robustly projecting the evolution of the OMZ for different O_2 thresholds is essential to assess ecological and climatic impacts. The expansion of Pacific suboxic waters ($O_2 < 5$ μmol/kg) could increase denitrification (nitrate-based respiration) and the subsequent production of nitrous oxide, a powerful greenhouse gas (Babbin et al., 2015; Yang et al., 2017). Yet, recent observational and modeling evidences suggest that half of the water column denitrification might occur in hypoxic waters with O_2 concentrations between 5 and 60 μmol/kg, due to the presence of low oxygen microenvironments in sinking particles (Bianchi et al., 2018), thus challenging the view that only suboxic waters should be considered when estimating nitrous oxide production. The expansion of hypoxic and low oxygenated waters would also threaten the habitat, diversity and survival of marine life (Levin, 2018), including species vital to local and global marine ecosystem services, such as anchovies, sardines, billfishes, and tunas (Bertrand et al., 2011; Chavez et al., 2008; Stramma et al., 2011). The lethal O_2 levels for many marine macro-organisms are found in the hypoxic range, between 20 and 80 μmol/kg, depending on the species, the life-stage (larva, juvenile, adult) and other environmental factors such as temperature (Keeling et al., 2010; Miller et al., 2002; Vaquer-Sunyer & Duarte, 2008). These lethal levels, which correspond

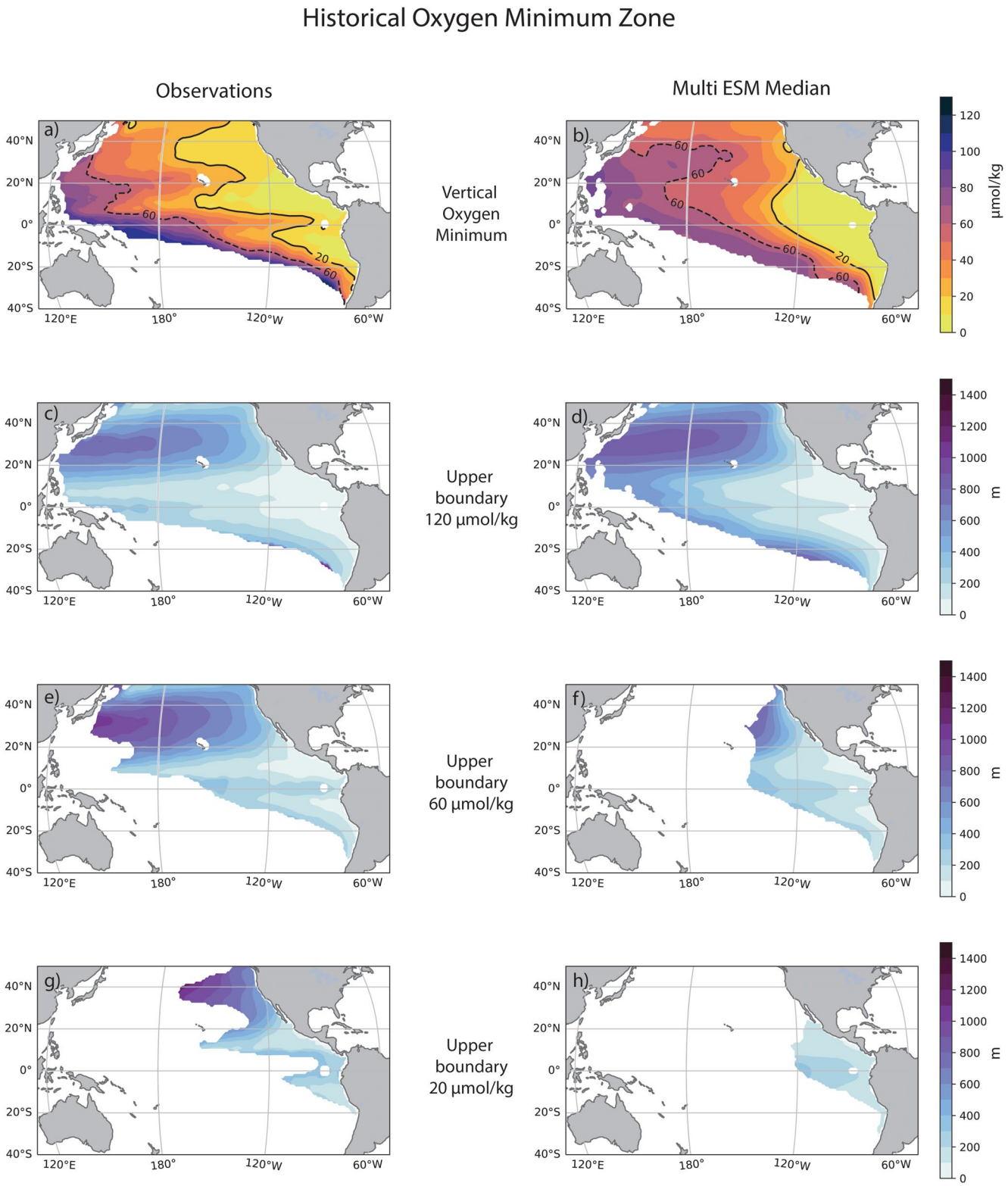
Historical Oxygen Minimum Zone
Observations
Multi ESM Median
Vertical Oxygen Minimum
Upper boundary 120 µmol/kg
Upper boundary 60 µmol/kg
Upper boundary 20 µmol/kg
a)
b)
c)
d)
e)
f)
g)
h)
40°N
20°N
0°
20°S
40°S
120°E
180°
120°W
60°W
60
20
µmol/kg
m
0
20
40
60
80
100
120
200
400
600
800
1000
1200
1400

Figure 1.

to the O_2 concentration required for survival in a resting state, are however generally a factor of 2–4 lower than the O_2 levels required to sustain the active aerobic activity (reproduction, swimming, feeding etc.) of these organisms (Deutsch et al., 2020). For instance, the optimum habitat of several valuable commercial fishes has been defined as $O_2 > 150$ µmol/kg. Sardines are found primarily offshore of the productive Peruvian coastal upwelling where O_2 concentrations exceed 150 µmol/kg despite lower food availability and eggs/larvae retention (Bertrand et al., 2011). Similarly, billfishes with tracking systems are found in waters with O_2 concentrations above 150 µmol/kg, only occasionally diving in waters with concentrations below that threshold (Stramma et al., 2011). Although the fate of these low oxygenated waters has often been overlooked, it is paramount to evaluate the impact of deoxygenation on ecosystems.

In this study, we investigate forced changes in the tropical Pacific Ocean OMZ and examine the potential physical and biological drivers of these changes using the latest generation of ESMs (CMIP6). We use a range of oxygen thresholds between 5 and 160 µmol/kg to define the OMZ (i.e., the volume of water with oxygen concentrations lower than a given threshold). This "oxygen framework" provides a more dynamically relevant perspective across ESMs than considering the OMZ over a fixed depth range (e.g., subsurface between 100 and 600 m) and a unique oxygen threshold to define its boundaries (e.g., O_2 below 60 µmol/kg), which might arbitrarily cut different dynamical regions of the OMZ in different ESMs. We consider a broad range of oxygen thresholds including suboxic, hypoxic and low oxygenated waters relevant for ecosystems, nitrogen dynamics and climate. We show that the projected fate of the OMZ falls into three regimes: (a) a robust expansion of low oxygenated waters due to reduced ventilation (OMZ defined by O_2 thresholds between 100 and 160 µmol/kg), (b) a slight contraction of the OMZ core likely due to changes in turbulent mixing and biological activity (O_2 thresholds of 20 µmol/kg and below), and (c) near-zero change in volume of hypoxic waters in between but potentially associated with a spatial redistribution of hypoxic waters (O_2 thresholds between 20 and 100 µmol/kg). We also discuss how this relatively consistent picture across ESMs clarifies the results of previous work on OMZ projections and discuss the potential impacts for ecosystems and nitrous oxide production.

2. Methods

2.1. CMIP6 Earth System Models and Observations

We use 14 ESMs from the CMIP6 archive that provide monthly outputs of ocean oxygen and meridional velocity for the preindustrial control, the historical period, and the high-emission scenario SSP5-8.5 (O'Neill et al., 2016) via the Earth System Grid Federation (Petrie et al., 2021). Our results consider the period from 1850 to 2100. We used additional variables that were not available for all of the ESMs: particulate carbon export at 100 m (*epc*100; available for 13 ESMs) as an indicator of biological processes, and ideal water age (variable *agessc*; available for 10 ESMs) as an indicator of circulation changes. We disregarded the ideal age from 3 ESMs (MPI-ESM1-2-HR, MRI-ESM2-0, and UKESM1-0-LL) and some members of MPI-ESM1-2-LR in which *agessc* was re-initialized to zero at the beginning of the historical and/or the SSP5-8.5 simulations as these could not be used to evaluate the changes in watermass age. For details on models and variable availability see Table 1.

We developed and used the "xMIP" python package (Busecke et al., 2022) to preprocess the CMIP6 ESM data (e.g., homogenize naming, units, and metadata/reconstruct missing grid metrics/masking ocean basins) in conjunction with a custom "intake-esm" (Banihirwe et al., 2020) catalog, which enables easy management of the large amount of data used in this study (100+ TB). To reduce the effects of model drift, we remove the linear trend of the preindustrial control run (starting at the branching point for each historical run) at every grid point for each ESM member. Most variables are provided on the ESM native grid (noted gn in Table 1). Some ESMs do, however, provide a subset of variables on a coarser $1° \times 1°$ grid (noted gr in Table 1). In these instances, we bilinearly interpolate the coarser values onto the higher resolution native grid using the "xESMF" python package (Zhuang et al., 2021), so that all variables are analyzed on the same grid for each ESM (see Table 1).

Figure 1. Historical (1950–2000) oxygen minimum zone (OMZ) in the tropical Pacific Ocean. Vertical minimum in oxygen concentration in (a) observations and (b) the Earth system model (ESM) ensemble median. Black lines indicate 20, 60, and 120 µmol/kg O_2 contours. Depth of the OMZ_{120} upper boundary ($O_2 = 120$ µmol/kg) in (c) observations and (d) the ensemble median. Depth of the OMZ_{60} upper boundary ($O_2 = 60$ µmol/kg) in (e) observations and (f) the ensemble median. Depth of the OMZ_{20} upper boundary ($O_2 = 20$ µmol/kg) in (g) observations and (h) the ensemble median. In all panels, values are smoothed using a 1° Gaussian filter. For the maps c-h, the median is only shown where more than 10 ESMs simulate the OMZ of for that particular threshold to avoid having the median map biased toward the few ESMs with unrealistically large OMZs (see Figures S3 and S4 in Supporting Information S1). Observations are from Bianchi et al. (2012).

Table 1
Earth System Model Data Used in This Study

ESM	Variables	Number of members
ACCESS-ESM1-5 (Ziehn et al., 2019a, 2019b)	agessc, epc100, o2, vo	3
CNRM-ESM2-1 (Seferian, 2018, 2019)	epc100, o2, vo	5
CanESM5 (Swart et al., 2019d, 2019e)	agessc, epc100, o2, vo	17
CanESM5-CanOE (Swart et al., 2019b, 2019c)	agessc, epc100, o2, vo	3
GFDL-CM4 (Guo et al., 2018a, 2018b)	agessc* (yr), o2 (gr), vo	1
GFDL-ESM4 (Krasting et al., 2018; John et al., 2018)	agessc* (yr), epc100 (gr), o2 (gr), vo*	1
IPSL-CM6A-LR (Boucher et al., 2018, 2019)	agessc, epc100, o2, vo	6
MIROC-ES2L (Hajima et al., 2019; Tachiiri et al., 2019)	agessc, epc100, o2, vo	1
MPI-ESM1-2-HR (Jungclaus et al., 2019; Schupfner et al., 2019)	epc100, o2, vo	2
MPI-ESM1-2-LR (Wieners et al., 2019a, 2019b)	agessc, epc100, o2, vo	10
MRI-ESM2-0 (Yukimoto et al., 2019a, 2019b)	epc100, o2, vo	1
NorESM2-LM (Seland et al., 2019a, 2019b)	agessc (gr), epc100, o2 (gr), vo	1
NorESM2-MM (Bentsen et al., 2019a, 2019b)	agessc (gr), epc100, o2 (gr), vo	1
UKESM1-0-LL (Tang et al., 2019; Good et al., 2019)	epc100, o2, so, thetao, vo	1

Note. Variables used: Dissolved oxygen concentration (O2), salinity (so), potential temperature (thetao), mixed layer depth (mlotst), particulate carbon export at 100 m (epc100), and ideal age (agessc) where available. We only use members that provide all data and can be detrended (some members could not be detrended due to errors in the metadata). The number of members used here can therefore be lower than the number published by the modeling center on Earth System Grid Federation (ESGF). If not otherwise marked variables are given as monthly averages on the native ocean grid of the respective ESM. Variables with "gr" were only available as regridded 1° by 1° outputs and have been bilinearly interpolated on the native grid to stay consistent with the other variables of that ESM. Variables with "yr" were only available as yearly output and were interpolated linearly to monthly intervals before analysis. Variable marked with an asterisk (*) are not available via ESGF and were provided by GFDL collaborator Jasmin John.

We used observations of dissolved oxygen concentrations from Bianchi et al. (2012), which is based on the World Ocean Atlas WOA05 (Garcia et al., 2006) but improves the representation of very low oxygen value. For comparison to observations, historical means for ESMs are computed as averages from 1950 to 2000. To calculate results from the ESM ensemble, we use a mean over members for each ESM, then a median over the ensemble. To quantify the uncertainty or spread on ensemble median quantities, we present an interquartile (IQ) range as the 25th and 75th percentile values in brackets. If not otherwise mentioned, the analysis (average, median, integrals, etc.) is performed for the Tropical Pacific (30°S–30°N).

2.2. The OMZ in Oxygen Coordinates

The OMZ is commonly defined as the ocean volume with oxygen concentration below a certain threshold $O_{2,0}$ as

$$\mathrm{OMZ}_{O_{2,0}} = \iiint_{O_2 <= O_{2,0}} dV \tag{1}$$

where the threshold values ($O_{2,0}$) vary. For this study we use an oxygen framework that examine the OMZ volume between thresholds from 5 to 160 µmol/kg and focus on three particular thresholds to illustrate changes: the OMZ core defined by a threshold $O_{2,0}$ = 20 µmol/kg (noted OMZ_{20}), hypoxic waters defined by a threshold $O_{2,0}$ = 60 µmol/kg (noted OMZ_{60}), and the low oxygenated waters using $O_{2,0}$ = 120 µmol/kg (noted OMZ_{120}).

We diagnosed vertical thickness and volume by converting O_2 values into µmol/kg using a constant reference density of ρ_0 = 1,025 kg/m^3 and calculate the sum of grid-cell volumes for each oxygen threshold with the "xhistogram" (R. Abernathey et al., 2021) python package (which enables the tracer dependent sum of grid cell volumes as an efficient and convenient operation on xarray datastructures). We use the full vertical column oxygen fields to compute the volume of the OMZ. The upper/lower boundary are found by linear interpolation using the oxygen concentration above/below the vertical oxygen minimum. OMZ thickness at each point in space is defined as the difference between lower and upper boundary.

When examining changes in particulate export as an indicator of biological processes, we considered export changes at 100 m depth averaged over the entire Tropical Pacific (30°S–30°N) and averaged over the area of the OMZ core. The changes over the entire Pacific likely influence the oxygen demand along the pathways of the subtropical cells that ventilate low oxygenated waters (OMZ_{120}) and to a lesser extent hypoxic waters (OMZ_{60}). In contrast, since advection is weak in the core (Lévy et al., 2021), we can assume that local sinking particles are the main contributor to the oxygen consumption in the core (OMZ_{20}). We defined this core mask over all horizontal grid cells of each individual ESM whose column contains the OMZ core for any year between 2000 and 2100.

2.3. Changes in Saturation and Apparent Oxygen Utilization

In order to attribute drivers of oxygen change in each model, we isolate the volumes ΔV_i over which the OMZ boundaries change during the twenty-first century at each oxygen threshold, that is, the volume that was either gained or lost between the historical mean (1950–2000) and the mean over the last 20 years of the SSP5-8.5 experiment (2080–2100). These ΔV_i partition the changes in OMZ volume into "nested shells layers." We decompose changes in oxygen concentration (ΔO_2) into changes in saturation concentration (ΔO_{2sat}) and in apparent oxygen utilization (AOU) at each gridcell:

$$\Delta O_2 = \Delta O_{2sat} - AOU \tag{2}$$

We then average these components over each of the volumes, ΔV_i. We calculate O_{2sat} from monthly average temperature and salinity fields using the gsw-python package (Firing et al., 2021), and AOU is calculated as the residual of the saturated and simulated states ($\Delta O_{2sat} - \Delta O_2$).

2.4. Subtropical Overturning Circulation and Subtrotropical Cell Index

To evaluate the large scale changes in the Pacific Ocean subtropical circulation we use the Subtropical Cell Index (STCI; Duteil et al., 2014) which quantifies the volume transport from the subtropics into the equatorial area in both hemispheres as:

$$STCI = \Psi_{max} - \Psi_{min} \tag{3}$$

with Ψ_{max} and Ψ_{min} the maximum and minimum of the volume overturning streamfunction Ψ in the upper 250 m and between 10°S and 10°N in the Pacific basin. Ψ at a latitude y and depth z is reconstructed as:

$$\Psi(y,z) = -\int_{z_0}^{z}\int_{x} v\left(x,y,z'\right)\, dx\, dz' \tag{4}$$

where z_0 is the ocean surface, and monthly meridional velocity v is linearly interpolated to a 1/4° by 1/4° for the Pacific Basin only. To focus on large-scale patterns, we smoothed the Ψ with a ~2° latitudinal filter.

3. Results

3.1. Historical Pacific OMZ Spatial Distribution and Geometry

The observed distributions of low oxygenated waters (OMZ_{120}) and hypoxic waters (OMZ_{60}) show a strong asymmetry between the Northern Hemisphere, where they extend to the western side of the basin, and the Southern Hemisphere where they are confined to the east (Figure 1a). The OMZ core (OMZ_{20}) also shows a strong north-south asymmetry, as it extends to about 160°W in the Northern Hemisphere but only to about 120°W in the Southern Hemisphere (yellow area in Figure 1a). A characteristic of the Pacific OMZ is the presence of higher O_2 concentrations along the Equator compared to concentrations on either side, leading to the equatorial separation of the core (Figure 1a). The ESM ensemble captures the north-south asymmetry in low oxygenated and hypoxic waters, with more than 10 of the ESMs representing the volumes of OMZ_{120} and OMZ_{60} that extend across the basin in the Northern Hemisphere but sharply retreat eastward in the Southern Hemisphere (Figure 1b). The north-south asymmetry of the OMZ core, as well as the separation of the core at the Equator are, however, underestimated (Figures 1a and 1b). We note in particular that OMZ_{20} does not extend north of 30°N in the ensemble median, potentially due to biases in the oxygenation of Pacific intermediate waters which form in the Bering and Okhotsk Seas and control the OMZ ventilation in this region (Bao & Li, 2016). Note, however,

that our analysis focuses on the tropical Pacific OMZ equatorward of 30° of latitude and does not include this region. All 14 ESMs in this study simulate low oxygenated, hypoxic and OMZ core waters in the tropical Pacific, but their spatial extent varies considerably across ESMs (Figures S1–S4 in Supporting Information S1). These differences in the representation of the OMZ north-south asymmetry and equatorial separation are largely tied to ESM differences in the ventilation pathways from subtropical and subpolar subduction and the Equatorial current, specifically the Equatorial Undercurrent (EUC) which carries oxygen eastward along the Equator, the alternating jets transporting low oxygen OMZ waters westward on either side of the EUC (Busecke et al., 2019; Harper, 2000; Llanillo et al., 2018; Margolskee et al., 2019; Stramma et al., 2010), as well as equatorial deep jets (Duteil et al., 2021). We find that ESMs with a more pronounced and more realistic equatorial separation of the OMZ are also ESMs in which the OMZ extends further west on either side of the Equator (ACCESS-ESM1-5, GFDL-ESM4, GFDL-CM4, MPI-ESM1-2-HR, MPI-ESM1-2-LR, NorESM2-MM, NorESM2-LM, see Figures S1–S4 in Supporting Information S1).

We further evaluate the geometry of the OMZ using the minimum depth of low oxygenated, hypoxic, and core waters across the Pacific Ocean (Figures 1c–1h). The observed OMZ_{120} upper boundary largely follows the structure of the thermocline. It is shallowest in the eastern equatorial Pacific (less than 100 m deep) and deepens westward and poleward into the subtropical gyres (400–800 m, Figure 1c). The ESM ensemble captures the shallow OMZ_{120} boundary in the eastern Pacific, but shows deeper values in the western tropical Pacific (600–1,500 m, Figure 1d). This deep bias in the ensemble median is caused by 6 ESMs that show an unrealistic deepening of the upper OMZ boundary between 120°W and 180°W (IPSL-CM6A-LR, CanESM5, CanESM5-CanOE, MRI-ESM2-0, MPI-ESM1-2-LR, MIROC-ES2L, see Figure S2 in Supporting Information S1). The depth of the OMZ_{20} upper boundary shows two distinct shallow lobes (100–200 m depth) extending to about 160°W at 10°N and about 120°W at 10°S (Figure 1g). The ensemble median simulates a two-lobe structure but underestimates its amplitude and, as mentioned above, does not capture the core north of 30°N (Figures 1g and 1h). Seven ESMs show a more realistic structure of the core upper boundary in particular its westward extension (ACCESS-ESM1-5, GFDL-CM4, GFDL-ESM4, NorESM-LM NorESM-MM, MPI-ESM1-2-LR, MPI-ESM1-2-HR), while 5 ESMs show a weak westward extension mirroring the ensemble median (CanESM5, CanESM5-CanOE, MIROC-ES2L, MRI-ESM2-0, UKESM1-0-LL, see Figure S3 in Supporting Information S1). The depth of the OMZ_{60} upper boundary expectedly falls in between the two end-members, and shares similar characteristics, including an underestimation of the equatorial separation and hemispheric asymmetry (Figures 1e and 1f).

Vertically, observations show that low oxygenated waters extend between 100 and 3,000 m depth with the bulk of the OMZ_{120} area located between 300 and 2,000 m (maximum area $>7.5 \times 10^{13}$ m^2, Figure 2c). The hypoxic waters are found between 100 and 2,000 m, with a maximum area located at around 500 m depth (maximum area $>4 \times 10^{13}$ m^2, Figure 2b). The OMZ core is even further limited in depth, and is located in the top 1,000 m with most of the OMZ_{20} area confined to 300–700 m depth (maximum area $>1.5 \times 10^{13}$ m^2, Figure 2a). The ensemble median captures relatively well the observed vertical distribution of the low oxygenated waters, although it overestimates the depth of the OMZ_{120} upper and lower boundary (Figure 2c). In contrast, the ESM ensemble overestimates the volume and vertical extent of the core and hypoxic waters. The area of the OMZ core is more than 50% larger in the ESM median than in observations below 1,000 m depth (area $>1 \times 10^{13}$ m^2 between 1,000 and 2,000 m, Figure 2a), and the area of hypoxic waters is more than 50% larger at 1,500 m depth and below (Figure 2b). We find a large spread across ESMs. Most ESMs simulate too deep OMZs, with OMZ_{120} that extend down to 4,000–6,000 m (MRI-ESM2-0, CNRM-ESM2-1 with OMZ area $>5 \times 10^{13}$ m^2 below 4,000 m, Figure 2c) and vast OMZ_{20} that extend even below 2,000 m (ACCESS-ESM1-5, GFDL-ESM4, MPI-ESM1-2-LR, MPI-ESM1-2-HR, NorESM2-LM, NorESM2-MM with core area $>1 \times 10^{13}$ m^2 below 2,000 m, Figure 2a), but a couple of ESMs simulate too shallow OMZs (UKESM1-0-LL and MIROC-ES2L with OMZ_{120} confined to the top 2,000 m, Figure 2c).

We extend the comparison of observed and simulated OMZ historical volumes to all oxygen thresholds between 5 and 160 μmol/kg (Figure 2d). The observed OMZ volume increases by about a factor of 4 from the OMZ core (1.2×10^{16} m^3 for OMZ_{20}, Table S1 in Supporting Information S1) to the hypoxic volume OMZ_{60} (4.6×10^{16} m^3; Table S2 in Supporting Information S1), and again by a factor of 4 from OMZ_{60} to OMZ_{120} (16.9×10^{16} m^3, Figure 2d, Tables S1–S3 in Supporting Information S1). The ensemble reproduces a slightly smaller increase in volume across thresholds (about a factor of 3 between both threshold pairs) and overestimates the OMZ volume across all oxygen thresholds (Figure 2d). Specifically, OMZ_{20} is over twice as large as in observations (2.5 vs. 1.2×10^{16} m^3) and the volume of OMZ_{60} and OMZ_{120} are 47% and 22% larger (6.7

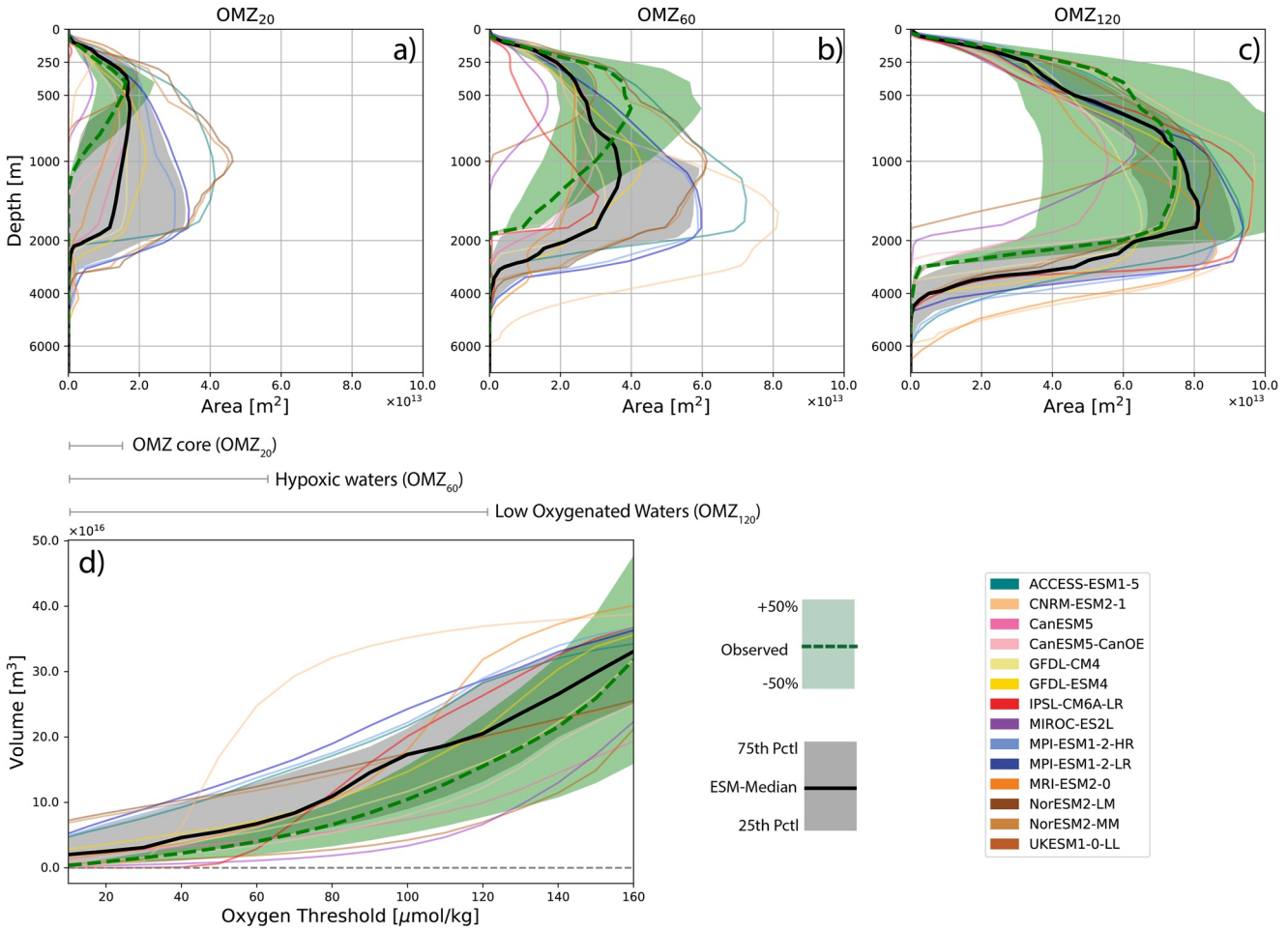

Figure 2. Historical (1950–2000) vertical area distribution (a) the oxygen minimum zone (OMZ) core (OMZ_{20}, $O_2 \leq 20$ μmol/kg), (b) hypoxic waters (OMZ_{60}, $O_2 \leq 60$ μmol/kg), and (c) low oxygenated waters (OMZ_{120}, $O_2 \leq 120$ μmol/kg). (d) OMZ volume as a function of the oxygen threshold for the multi-Earth system model (ESM) ensemble median (black line with first and third quartile interval as gray shading), and for observations from Bianchi et al. (2012) (dashed green line with green shading indicating ±50% of observed value). Colored lines show individual ESMs (mean of all members available for each ESM).

vs. 4.6×10^{16} m^3 and 20.6 vs. 17.0×10^{16} m^3, Figure 2d). There is again a wide spread across ESMs, with some ESMs capturing the OMZ volume within 50% percent of observations for most oxygen thresholds (e.g., GFDL-CM4,GFDL-ESM4 CanESM5-CanOE, and CanESM5), while others either underestimate the volume by more than 50% (MIROC-ES2L, UKESM1-0-LL) or overestimate it by more than 50% (MPI-ESM1-2-LR, MPI-ESM1-2-HR, ACCESS-ESM1-5, CNRM-ESM2-1) for most oxygen thresholds (Figure 2d).

3.2. Future OMZ Volume Changes

We examine projected changes in OMZ volume over the 21st century as a function of oxygen thresholds. The ESM ensemble suggests that the volume of loosely defined low oxygenated waters (O_2 thresholds of 100–160 μmol/kg) will expand, while the volume of OMZ core waters (O_2 thresholds of 20 μmol/kg or lower) might slightly shrink over the 2000–2100 period (Figure 3a). For instance, the ensemble median projects a robust increase of OMZ_{120} of about 4% (0.8 [0.6, 1.0] $\times 10^{16}$ m^3/century, ESM median and IQ range uncertainty), and a decrease of OMZ_{20} of about 4% (−0.1 [− 0.5, 0] $\times 10^{16}$ m^3/century) compared to the historical volume. At intermediate O_2 thresholds (20–100 μmol/kg), the ESM ensemble projects near-zero change as it transitions from the contraction of the core to the expansion of low oxygenated waters (see for instance OMZ_{60} change of 0.0 [−0.3, 0.1] $\times 10^{16}$ m^3/century). The expansion of low oxygenated waters is robust across the ESM ensemble (all 14 ESMs project an expansion for O_2 thresholds higher than 100 μmol/kg) and the projected magnitude of this expansion is relatively well constrained (IQ range of ±25%, see Table S3 in Supporting Information S1 for

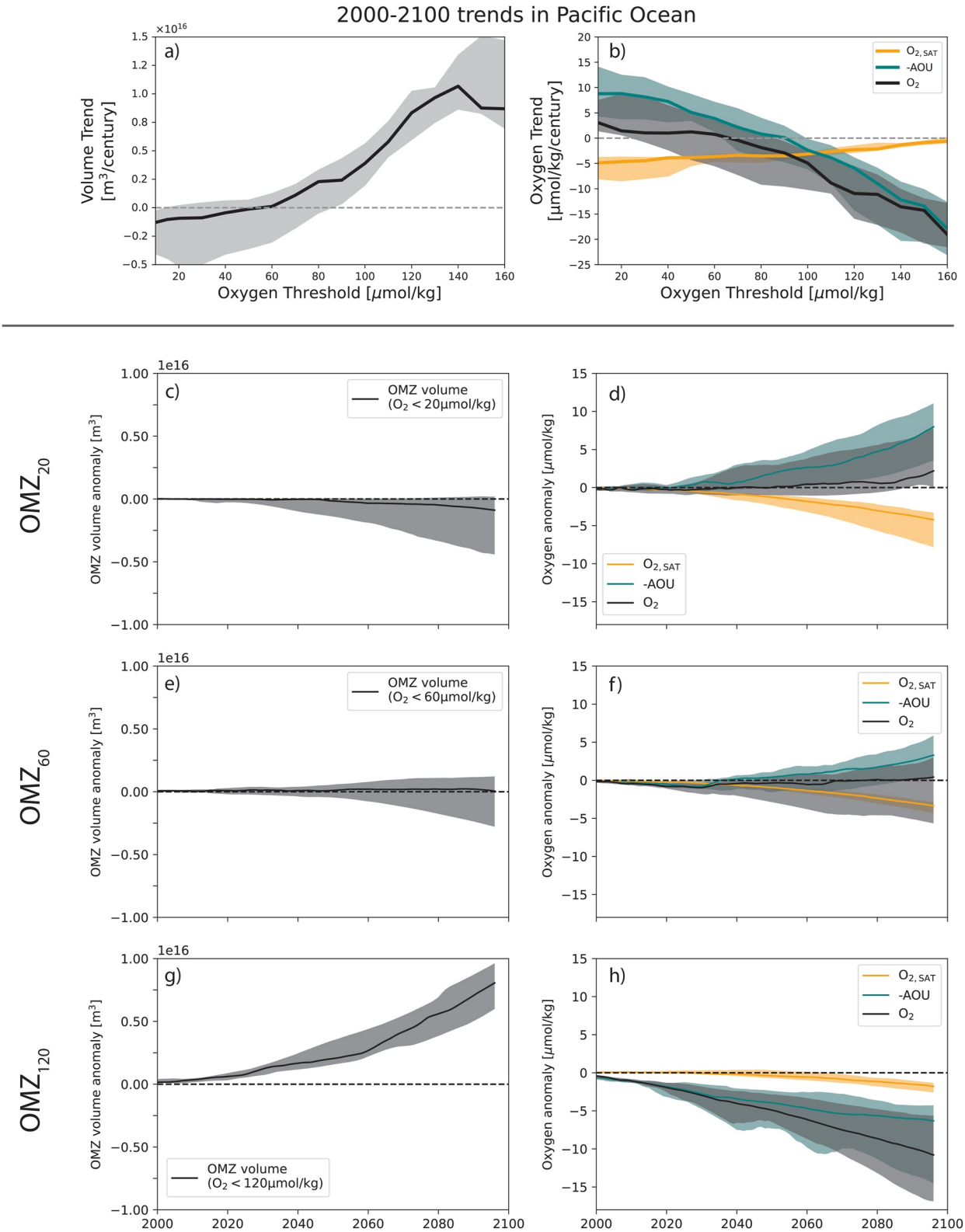

Figure 3. Projected changes in oxygen minimum zone (OMZ) volume (left) and oxygen concentrations (right) including contributions from thermal (O_{2sat}) and non-thermal (-AOU) changes in the tropical Pacific Ocean. Linear trends (2000–2100) in (a) OMZ volume and (b) oxygen concentrations as a function of oxygen thresholds. Timeseries for three thresholds: (c and d) the OMZ core (OMZ_{20}), (e and f) hypoxic waters (OMZ_{60}), and (g and h) low oxygenated waters (OMZ_{120}). In all panels, lines represent the Earth system model (ESM) median, and shading represents the interquartile range. Time-series of ESM anomalies are smoothed with a 10-year rolling average before taking ESM median.

individual models). The contraction of the core is more uncertain (7 out of the 14 ESMs simulate a contraction of OMZ_{20}, 4 ESMs simulate virtually no change and 3 ESMs simulate an expansion, Table S1 in Supporting Information S1) and its magnitude could be marginal (IQ range reaching 0 change). We note however that the 3 ESMs that show a significant expansion of core waters are the three ESMs with unrealistically small historical core volumes (CNRM-ESM2-1, IPSL-CM6A-LR, and MIROC-ES2L, Table S1 in Supporting Information S1). The transition from contraction to expansion makes projection of the hypoxic range difficult to assess, specifically because this transition occurs at different thresholds for the different ESMs. For instance, the volume of OMZ_{60} expands in 5 ESMs, contracts in 4 ESMs and experiences near-zero change in 5 ESMs (Table S2 in Supporting Information S1). The proportion of ESMs that expand would, however, be lower for a threshold of 40 µmol/kg and higher for a threshold of 80 µmol/kg. This transition regime likely explains the large uncertainties found in prior work that specifically targeted hypoxic thresholds (e.g., Bopp et al., 2013; Cabré et al., 2015; Cocco et al., 2012; Shigemitsu et al., 2017).

3.3. Non-Thermal Changes Dictate Expansion and Contraction Regimes

The expansion of the low oxygenated waters is consistent with the widespread loss of O_2 simulated by the ESMs (−2 to −20 µmol/kg from 2000 to 2100, Figure 4a), and the contraction of the core is consistent with the weak gain in O_2 simulated in the eastern Pacific, where the boundaries of OMZ_{20} are located (up to +2 µmol/kg from 2000 to 2100 average across the eastern Pacific, Figure 4a). We show a meridional section in the central Pacific, which reveals that the O_2 loss is most intense along the bowl-shaped ventilation pathway associated with the subtropical cells, and more specifically the northern cell (Figure 4e). As a result, the upper boundary of OMZ_{120} shallows by about 200 m in the north of this region (from black to gray contours, Figure 4e). This section also shows that oxygen changes simulated by the ESM median at the OMZ_{60} boundary are not significant (stippling) except along the northern subtropical cell pathway (25°–30°N), and in the region of the northern subsurface countercurrent (westward current at ∼8°N, 250–500 m depth). Note that the signature of the subsurface countercurrent in the ESM median comes from a few ESMs that resolve the east/west alternating jets in the Equatorial region (MPI-ESM1-2-HR, GFDL-ESM4, GFDL-CM4, NorESM2-MM, Figure S9 in Supporting Information S1). The slight expansion of OMZ_{60} in these two regions suggest that some contraction and spatial redistribution of the OMZ_{60} volume occurs elsewhere in the tropical Pacific to yield the virtually zero change projected by the ESM median (Figures 3a, 3e and 4e). This is confirmed by a section in the eastern Pacific (Figure 4i) which shows a slight expansion of OMZ_{60} at ∼10°S and 250 m depth. This eastern Pacific section also shows that the contraction of the core occurs at both the upper and lower boundary due to an increase in O_2.

We can decompose the changes in oxygen into contributions from thermally driven changes in oxygen saturation (O_{2sat}), and non-thermal changes tied to circulation and biological activity, combined together using AOU ($-AOU = O_2 - O_{2sat}$, see Section 2). The ESM median projects negative changes in O_{2sat} consistent with a warming of the upper ocean and the penetration of surface warmer waters into the ocean interior along the pathways of the subtropical cells (Figures 4b, 4f and 4j). These changes in O_{2sat} contribute to the deoxygenation in the upper 750–1,000 m, but cannot explain the magnitude of the O_2 loss along the subtropical cells and the contrasting O_2 gain toward the OMZ core (Figure 4). Changes in AOU act to increase O_2 toward the core, and to reduce O_2 along the bowl-shaped subtropical cell pathways (Figures 4c and 4g), indicating that changes in circulation and biology control the spatial contrast in oxygen change and the diverging fates of OMZ_{20} and OMZ_{120}.

We further quantify the contribution of thermal and non-thermal processes to the change in OMZ volume by computing changes in O_2, O_{2sat} and AOU within the OMZ volume that was gained or lost between 2000 and 2100, and apply this "nested shell layers" decomposition to the different OMZ thresholds (see Section 2). The contraction of the OMZ_{20} volume by 2100 (-0.1×10^{16} m^3, Figure 3c) is associated with an increase in O_2 of 1.4 µmol/kg in the OMZ_{20} volume that was lost ([0.6, 8.8] µmol/kg). This oxygenation of the core outer layer arises from a non-thermal (−AOU) increase in O_2 of 8.8 µmol/kg ([3.7, 12.5] µmol/kg), partly offset by a reduction in O_{2sat} of −4.6 µmol/kg ([−8.5, −3.6] µmol/kg, Figure 3d). The expansion of the low oxygenated waters (0.8×10^{16} m^3, Figure 3g) is also largely controlled by non-thermal changes, but in this case both the non-thermal (−5.9 [−14.3, −3.8] µmol/kg) and thermal (−2.3 [−2.9, −1.4] µmol/kg) changes act to reduce O_2 concentrations in the OMZ_{120} volume that was gained (Figure 3h). In between, the volume of hypoxic waters OMZ_{60} is relatively stable due to the near complete compensation between non-thermal and thermal changes (Figures 3e and 3f).

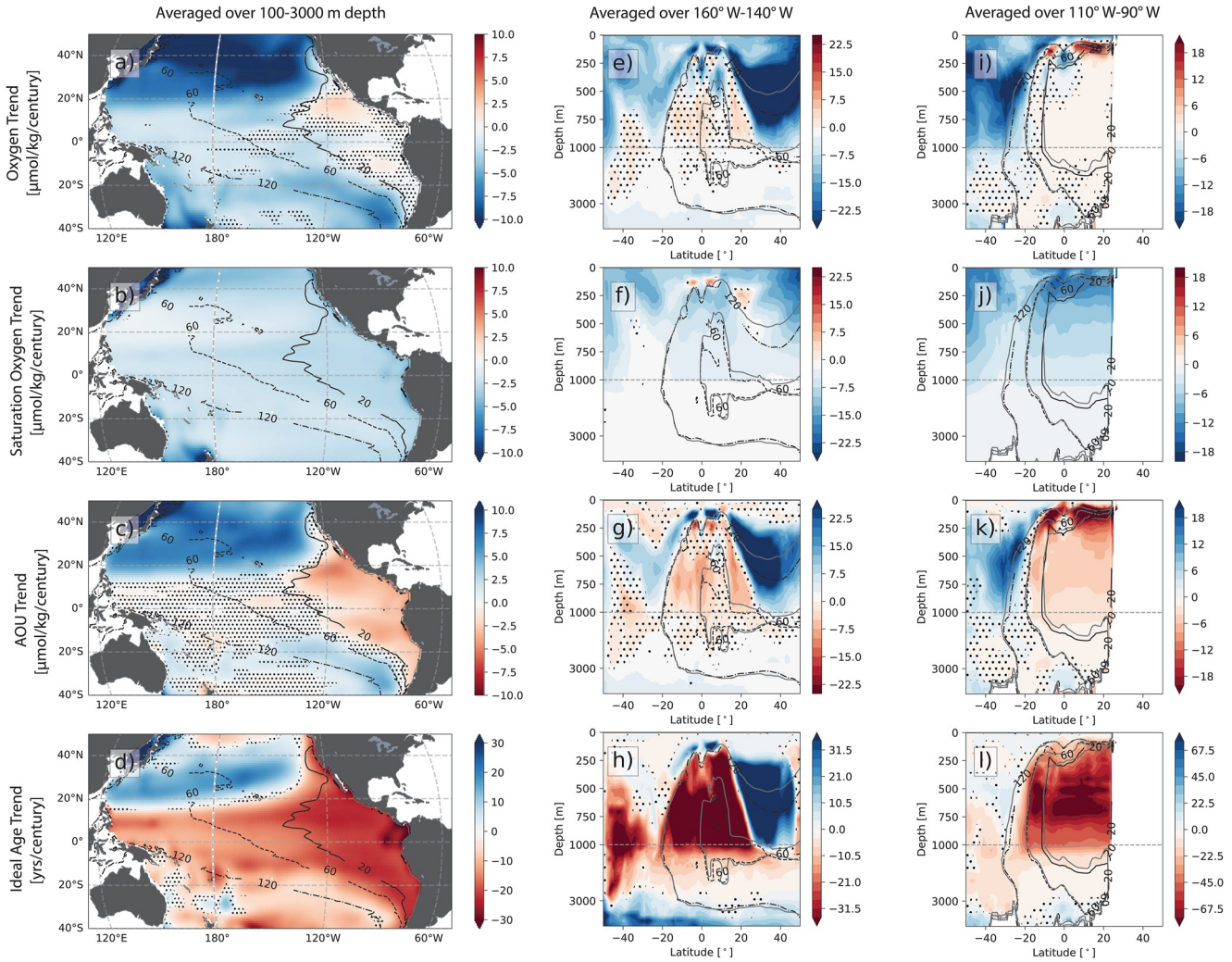

Figure 4. Projected changes (2000–2100) averaged in the main oxygen minimum zone (OMZ) depth range (100–3,000 m, see Figure 2a) for: (a) oxygen concentrations, (b) oxygen saturation concentrations (O_{2sat}), (c) apparent oxygen utilization, and (d) ideal age (10 Earth system models [ESMs] available). All fields are spatially smoothed using a 1° Gaussian filter. (e–l) Vertical sections of the simulated changes averaged between (e–h) 160°–140°W, and (i–l) 110°–90°W for the same tracers. Changes are computed as linear trends over 2000–2100 and shown as ensemble median. Dotted areas indicate where less than 60% of the ESMs agree on the sign. On panels (e–l), black contours indicate the extent of the 120, 60, and 20 µmol/kg waters averaged from 1950 to 2000, and gray contours their extent at the end of the century (added linear change from 2000 to 2100). Note that some colorbars are flipped so colors match the anticipated effect on oxygen (e.g., an increase in age is expected to result in a decrease in oxygen). Sections for individual ESMs are in Figures S9 and S10 in Supporting Information S1.

We generalize this thermal/non-thermal decomposition to all OMZ thresholds between 5 and 160 µmol/kg (Figure 3b). Non-thermal changes dictate the transition from core contraction for thresholds lower than 20 µmol/kg to expansion for thresholds higher than 100 µmol/kg (Figures 3a and 3b). The contribution of non-thermal processes evolves from a maximum oxygenation of +8.8 [4.3, 14.1] µmol/kg/century for suboxic waters (threshold of 5 µmol/kg) to a maximum de-oxygenation of −17.9 [−23.1, −12.6] µmol/kg/century for the highest OMZ threshold (160 µmol/kg, Figure 3b). In contrast, changes in O_{2sat} lead to an oxygen loss and act to expand the OMZ volume across all thresholds (Figure 3b). This thermal loss partly offsets the non-thermal oxygenation for thresholds lower than 20 µmol/kg, largely cancels the non-thermal oxygenation for thresholds between 20 and 100 µmol/kg, and slightly reinforces the non-thermal deoxygenation for thresholds above 100 µmol/kg. We note that the spread between ESMs is substantially smaller for changes in O_{2sat} than for AOU, and that the uncertainty in the sign of the OMZ projection, particularly the fate of hypoxic waters at intermediate thresholds (40–100 µmol/kg), is mostly associated with uncertainties in non-thermal biological and/or circulation changes (Figure 3a).

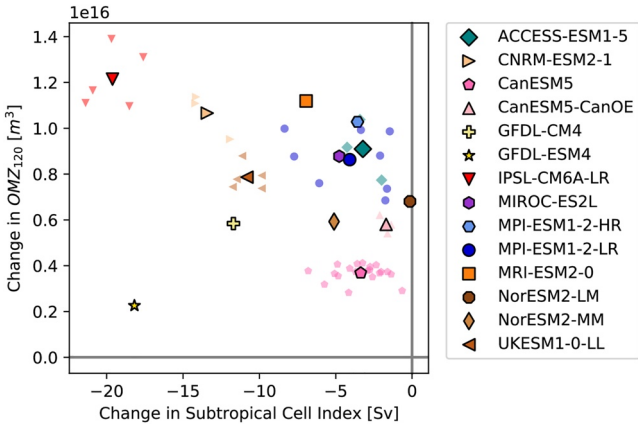

Figure 5. Relationship between changes (linear trend over 2000–2100) in OMZ_{120} volume (m^3) and Subtropical Cell Index (Sv) (Duteil et al. (2014); see Section 2). Earth system model (ESM) members are shown as transparent circles, with the member mean as filled black circles.

3.4. Role of Ocean Circulation and Biological Activity

We examine the processes responsible for the spatial pattern in non-thermal oxygen changes (AOU pattern) that control the contrasting behavior between the expansion of low oxygenated waters and the contraction of the OMZ core. Oxygen budget terms are not available in the CMIP6 archive, but we provide a qualitative assessment and discuss the changes in oxygen supply and biological demand, using changes in the ideal age tracer (available for 10 out of 14 ESMs) and particle export at 100 m depth (available for 13 out of 14 ESMs). The assumption is that increased water age indicates a decrease in ventilation and oxygen concentrations, while reduced export yields reduced respiration and oxygen consumption at depth (i.e., increase in O_2 concentrations). We restrict our qualitative discussion to the two end-members, the OMZ core and low oxygenated waters.

3.4.1. Weaker Ventilation Controls the Expansion of Low Oxygenated Waters

The ESM ensemble robustly projects decreasing O_2 levels along the circulation pathways of the subtropical cell (upper 200–1,000 m, shoaling toward the Equator; Figures 4e and 4g), which ultimately drive the expansion of the low oxygenated water volume (see Section 3.4.1). These changes are collocated with increasing ideal age (i.e., the time since the water mass was last in contact with the atmosphere increases; Figure 4h), suggesting that the expansion of low oxygenated waters is caused by a basin-scale weakening of the ocean circulation. This is further supported by the link found between the volume of low oxygenated waters and the strength of the subtropical cells that transport oxygenated waters from the subtropics to the OMZ periphery (Figure 5). The OMZ_{120} volume expands as the STCI (an indicator of the strength of the subtropical cells) weakens. This result is consistent with the work of Duteil et al. (2014) who identified a strong link between changes in upper ocean O_2 and shallow overturning circulation in the tropical Pacific Ocean since the 1960s using an ocean bio-physical model.

Changes in biological activity cannot explain the oxygen loss in subtropical cell waters. Indeed, all ESMs project a basin-scale decline in particulate export in the tropical Pacific Ocean, ranging between −4% and −50% (Figure 6c), which likely reduces respiration and O_2 consumption at depth (basin-scale export changes are relevant here because they control the oxygen consumption in the water masses that ventilate the vast volume of low oxygenated waters). This basin-scale weakening in export production is in line with prior work that showed that increased stratification and weaker eddy turbulent mixing associated with global warming reduced the upward transport of nutrients that fuel biological production and O_2 consumption at depth (Couespel et al., 2019; Deutsch et al., 2014; Doney & Karnauskas, 2014; Duteil et al., 2014, 2018; Palter & Trossman, 2018). This change in biological demand is not consistent with the projected O_2 loss along the subtropical cell pathway and the expansion of low oxygenated waters (reduced export and biological demand alone would increase O_2 at depth). The reduction in biological oxygen demand might, however, offset part of the weaker supply of O_2 by ventilation and act as a stabilizing feedback on tropical O_2 levels and the volume of low oxygenated waters.

Age and basin-scale export only provide a qualitative assessment of circulation and biological changes. As a result, in the ESMs examined here we cannot quantify the magnitude of the compensation between changes in ventilation and respiration at depth, which would require a detailed O_2 budget. The very robust and consistent expansion of low oxygenated waters and large-scale O_2 decline projected by all ESMs strongly suggest, however, that changes in respiration are small compared to the weakening of the circulation. We thus conclude that changes in circulation, specifically the weakening of the subtropical cell, are the main driver of the projected expansion of low oxygenated waters.

3.4.2. Increased Ventilation and Reduced Biological Demand in OMZ Core

Our results suggest that both circulation and biological changes contribute to the projected contraction of the OMZ core. The OMZ core has no direct connection with advective ventilation pathways and is largely influenced by local changes in eddy turbulent mixing and biological consumption (Lévy et al., 2021). The ESMs simulate an increase in ideal age in the eastern Equatorial Pacific where the OMZ core is located and along the ventilation pathway of intermediate waters in the Southern Hemisphere (750–2,000 m depth, Figures 4h and 4l),

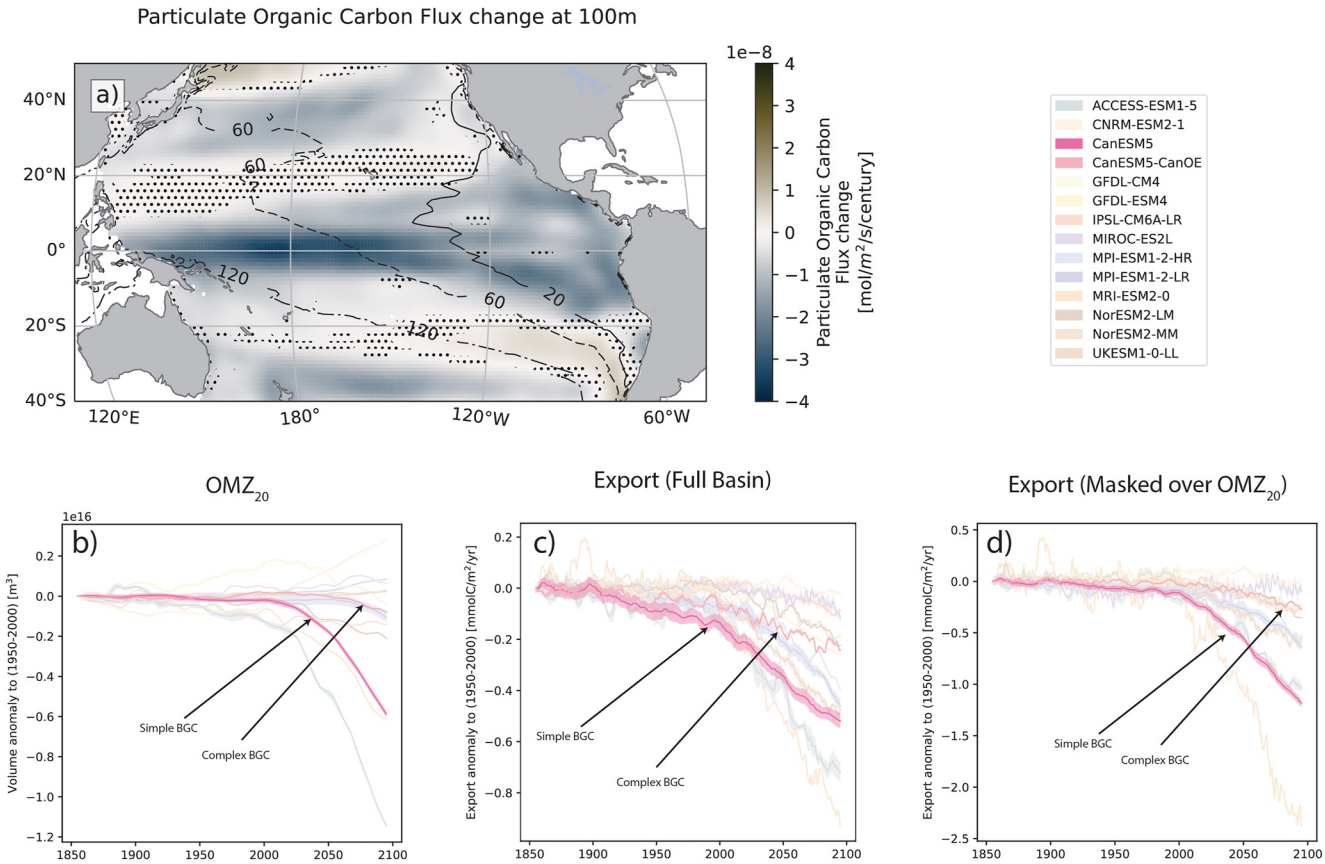

Figure 6. Changes in particulate organic carbon export at 100 m in Earth system model (ESM) median (13 ESMs available) overlaid with historical vertical minimum oxygen levels of 120, 60, and 20 μmol/kg (black contours). Dotted areas indicate where less than 60% of the ESMs agree on the sign and changes are computed as linear trends over 2000–2100. Time-series of ESM anomalies in (b) OMZ_{20} volume, (c) particulate organic carbon export at 100 m over the tropical Pacific Ocean (30°S–30°N), and (d) particulate organic carbon export at 100 m over the extent of the OMZ core of each individual ESMs (see Section 2 for details). Results from two ESMs with identical ocean physical module but different biogeochemical module (CanESM5 and CanESm-CanOE) are highlighted. Shading indicates standard deviation between ESM members when available. Values in panel (a) are spatially smoothed using a 1° Gaussian filter. Timeseries are smoothed with a 10-year rolling average.

suggesting faster renewal of intermediate waters and OMZ core waters. This agrees with prior modeling studies which identified that higher O_2 concentrations and younger ages in the Pacific Ocean shadow zones in future projections (also found in CMIP5 by Cabré et al. (2015)) were linked to changes in the renewal of intermediate waters (Gnanadesikan et al., 2012), and to changes in vertical and horizontal mixing which increased the relative contribution of younger upper ocean waters compared to older deeper waters (Bahl et al., 2019; Gnanadesikan et al., 2007). In addition to the faster renewal of core waters, the ensemble projects a consistent decrease in particulate export over the regions of the OMZ core in the eastern Tropical Pacific (Figure 6a), which would reduce the local O_2 biological demand and reinforce the effect of ventilation in reducing the core volume (local changes in export/remineralization are likely to contribute more than basin-scale changes at low oxygen thresholds, due to the higher residence time and absence of strong advection).

We cannot quantify the relative contribution of reduced biological demand compared to increased ventilation in the projected contraction of the OMZ core using currently available CMIP6 data, but we can explore the sensitivity of the biological changes using the two Canadian ESMs, CanESM5 and CanESM5-CanOE, which are identical except for the ocean biogeochemical module (Swart et al., 2019a). CanESM5-CanOE includes multiple food chains, a prognostic iron cycle, and prognostic denitrification, whereas CanESM5 simulates oxygen purely as a diagnostic or "downstream" tracer that does not affect other biogeochemical processes (Christian et al., 2022). We find that CanESM5-CanOE predicts a weaker export reduction (9% vs. 27% decrease in CanESM5, Figure 6c) and a weaker core contraction (10% vs. 29% decrease in CanESM5, Figure 6b). We only have one pair of ESMs in this comparison, and thus cannot make a general statement, but this particular case suggests that (a) changes in

export production and oxygen demand modulate the magnitude of the OMZ core contraction, and (b) including a more realistic description of the biogeochemistry stabilizes the OMZ core and ESMs with simple biogeochemical modules might overestimate the contraction of the core. An implication of this result is that the core volume might in fact be relatively stable even under strong anthropogenic forcing. We note however that confirming these findings in a more quantitative way using the full ESM ensemble would require additional outputs (oxygen sources and sinks), which should be considered for future model intercomparison projects. A better constraint on the influence of biology on the core contraction might improve agreement of the transition zone between contraction and expansion and thus the fate of hypoxic water volume in the future.

3.5. Shoaling of Low Oxygenated Waters and Deepening of the Core

Changes in OMZ volume directly influence its thickness and the depth of its upper boundary. The expansion of low oxygenated waters is associated with an increase in the OMZ_{120} thickness of 20–50 m and a shallowing of the OMZ_{120} upper boundary of 5–50 m over most of the Tropical Pacific, except in the eastern Pacific Ocean where a mild reduction of the OMZ_{120} thickness and a deepening of its upper boundary (both less than 8 m; Figures 7a and 7b) are collocated with the contraction of the OMZ core. Indeed, the ensemble projects that the two-lobe structure of the core (i.e., deeper core at the Equator with two shallower lobes off of the Equator, see Figure 1) will flatten in the future. As a result, OMZ_{20} would thin by about 10–30 m off of the Equator and thicken by about 5–20 m at the Equator, with the response off of the Equator controlling the projected overall core contraction (Figures 7e and 7f). These changes in thickness translate into a deepening of the OMZ_{20} upper boundary by 5–20 m off the Equator and a shallowing of the core upper boundary by up to 10 m at the Equator (Figure 7). Although there is no significant change in the OMZ_{60} volume, the ESM ensemble suggests there is some spatial redistribution in the volume of hypoxic waters (Figures 7c and 7d). This redistribution follows the patterns of expansion tied to the weaker subtropical cell ventilation and the contraction of the core. As a result, the upper boundary of OMZ_{60} deepens by about 5 m where the core expands and shallows by 5–30 m on its northern flank.

The amplitude of these changes differ substantially between ESMs and largely depend on the position of the historical OMZ in each ESM (Figures S6–S8 in Supporting Information S1). Yet, Figures 7g–7i shows that the local relationship (i.e., at each grid point) between OMZ thickness and upper boundary depth holds for the three thresholds (20, 60, and 120 µmol/kg) and all ESMs regardless of their OMZ shape. The depth of the upper boundary is expected to shoal (respectively deepen) by about 6 m when the OMZ thickens (respectively thins) by 10 m (slope of −0.56 to −0.62 m per meter of thickness increase; explained variance of 40%–55%). This suggests that about 60% of the local change in the OMZ_{120}, OMZ_{60}, and OMZ_{20} thickness would translate into a change in the upper OMZ boundary (the other 40% change influencing the lower boundary in the deep ocean).

4. Discussion and Conclusion

We used the latest CMIP6 ESM generation to investigate the future evolution of the Pacific OMZ. The results show that climate change under high greenhouse gas emissions (scenario SSP5-8.5) will very likely lead to an expansion of the volume of low oxygenated waters (oxygen thresholds between 100 and 160 µmol/kg), and might lead to a slight contraction of the OMZ core (oxygen thresholds lower than 20 µmol/kg) in the Tropical Pacific by the end of the 21st century. In between, the ESMs transition from contraction to expansion and project near-zero changes in the volume of hypoxic waters (oxygen thresholds between 20 and 100 µmol/kg). We find that oxygen saturation changes yield a relatively homogeneous basin-scale deoxygenation of the Tropical Pacific Ocean in agreement with prior studies (Bopp et al., 2002, 2013; Buchanan & Tagliabue, 2021; Kwiatkowski et al., 2020), while non-thermal changes dictate the transition from contraction to expansion. The expansion of low oxygenated waters is controlled by decreased ventilation, while the contraction of the core is influenced by both circulation (likely an increase in intermediate waters ventilation and changes in mixing ratios between young and older waters, Bahl et al., 2019; Gnanadesikan et al., 2007, 2012) and biological processes (reduced export production leading to less oxygen demand at depth).

The ESM ensemble indicates that the influence of ventilation changes on both the expansion of low oxygenated waters and the contraction of the core depends on the simulated OMZ historical distribution which can depart from the observed distribution. We note in particular some systematic biases across the ensemble: the core and

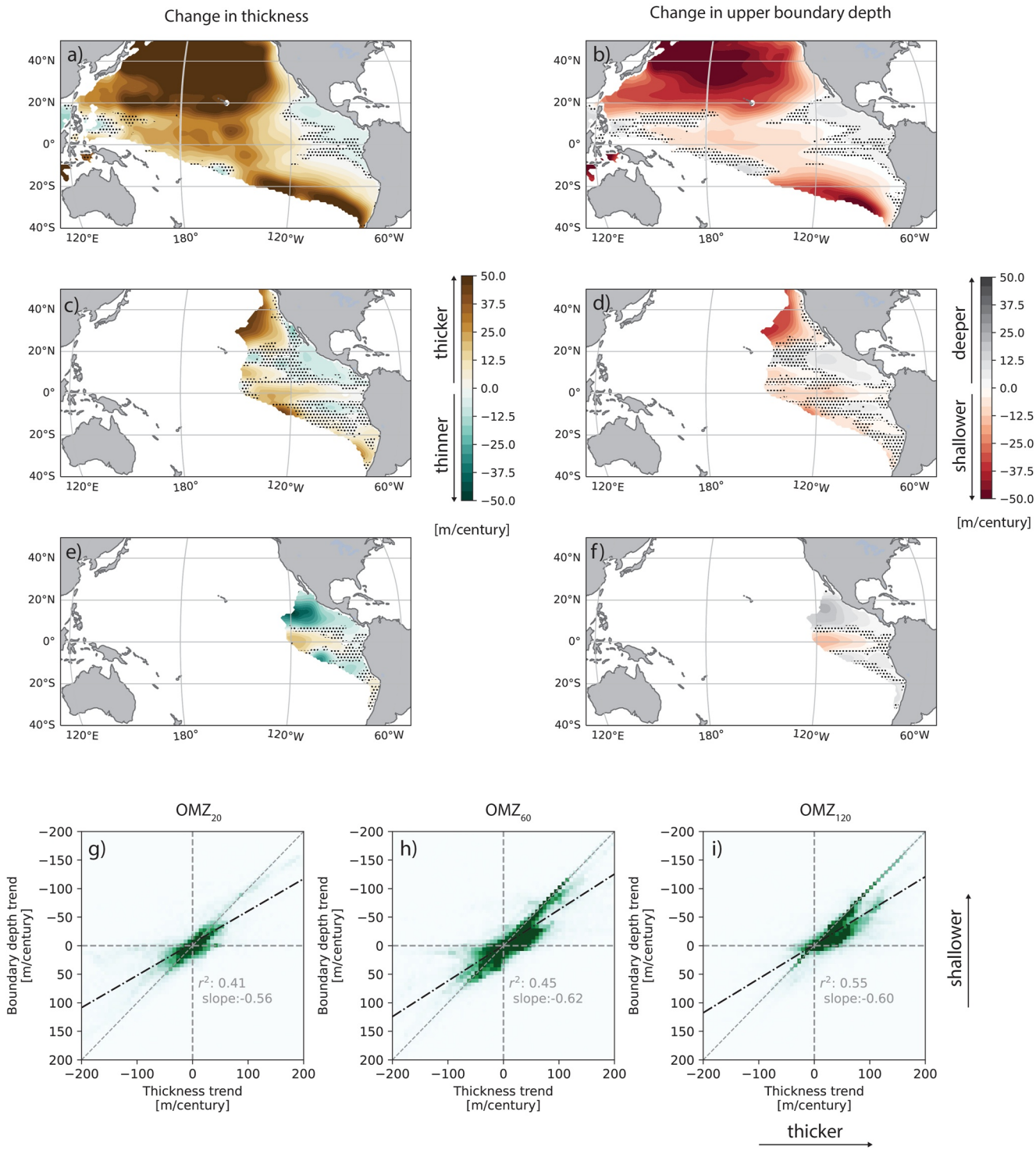

Figure 7. Changes in thickness and depth of upper boundary for (a and b) low oxygenated waters (OMZ_{120}), (c and d) hypoxic waters (OMZ_{60}), and (e and f) the OMZ core (OMZ_{20}). Changes are computed as linear trends over 2000–2100 and smoothed using a 1° Gaussian filter. Dotted areas indicate where less than 60% of the Earth system models (ESMs) agree on the sign. Local (at every grid-point) relationship between changes in thickness and the depth of the upper boundary for (g) OMZ_{120}, (h) OMZ_{60}, and (i) OMZ_{20}. Black dashed-dotted line indicates linear regression through all data points. Green color indicates relative density of grid-points within bins.

hypoxic waters are too deep in most models (Figure 2) and core waters are absent from many ESMs north of 30°N (Figure S1 in Supporting Information S1). The crucial role of ventilation highlighted here and in other studies (Bahl et al., 2019; Buchanan & Tagliabue, 2021; Busecke et al., 2019; Czeschel et al., 2010; Duteil et al., 2021; Gnanadesikan et al., 2007; Lévy et al., 2021; Margolskee et al., 2019; Palter & Trossman, 2018; Stramma

et al., 2010) strongly suggests that a better representation of the OMZ and its core hinges on tighter constraints of the subtropical cells and intermediate transport pathways from the subtropics and mid-latitude into the Tropical Pacific, including the alternating zonal jets which are often misrepresented in ESMs. Finally, a more quantitative assessment of physical and biological drivers across the ESM ensemble would require at least a subset of the oxygen budget terms (in particular the biological consumption term). While it will be prohibitively expensive to save full budget terms as monthly 3D fields, future model intercomparison projects might consider making long term averages (e.g., decadal) of oxygen budget terms available. This would certainly advance the understanding of long-term projected changes, hopefully leading to an improved representation of OMZs in general.

The consistency found in ESM projections using the oxygen framework provides context for previous work that showed inconsistent changes in tropical oxygen content and OMZ size (Bopp et al., 2013; Cabré et al., 2015; Kwiatkowski et al., 2020; Séférian et al., 2020; Shigemitsu et al., 2017). Differences between our results and prior findings can be explained by two factors. First, the representation of the OMZ has improved in many ESMs compared to the prior generation of ESMs used in most of these studies (Séférian et al., 2020), specifically the representation of the Equatorial current system (Karnauskas et al., 2020) which strongly affects the historical extent of the upper OMZ (Busecke et al., 2019). Second, our approach considers volume changes for different O_2 thresholds over the full water column. This framework allows one to capture the similarities of the OMZ dynamics in the different ESMs (e.g., advection controls ventilation at the OMZ periphery while mixing controls it in the core) despite ESM biases in the representation of the OMZ and core spatial distribution. Dynamically, regions with very low oxygen concentrations will always lie within the shadow zone of a specific ESM, while higher oxygen regions will lie in regions influenced by advective processes, regardless of existing biases in the historical geometry of the OMZ. This contrasts with prior works examining both CMIP5 ESMs (Cabré et al., 2015) and CMIP6 ESMs (Kwiatkowski et al., 2020) that concluded that changes in oxygen were inconsistent in the OMZ regions because they considered limited depth ranges (0–1,000 m for CMIP5 and 100–600 m for CMIP6) which excluded large parts of the OMZ and OMZ core (Figure 2). Here, we employ an O_2 framework over the full water column to reveal that behavior of the OMZ is relatively consistent across ESMs, but that the threshold at which the OMZ starts expanding varies between ESMs. This ESM sensitivity to the oxygen threshold (i.e., some ESMs expand for $O_2 \leq 50$ μmol/kg while others expand for $O_2 \leq 100$ μmol/kg) is likely related to their differences in historical oxygen distribution and OMZ spatial shape, with very different large scale gradients (Figure S1 in Supporting Information S1). Earlier studies have mostly used OMZ thresholds within this uncertain 20–100 μmol/kg range (50 μmol/kg in Cabré et al. (2015), 30 μmol/kg in Shigemitsu et al. (2017), and 50–80 μmol/kg in Bopp et al. (2013)). It is possible that applying a similar framework to previous ESM generations could reconcile some of the discrepancies found in OMZ projections.

The expansion of low oxygenated waters is relatively well constrained in the CMIP6 ESM ensemble (0.8×10^{16} m^3/century with an IQ range between 0.6 and 1.0×10^{16} m^3/century for OMZ_{120}), but some uncertainties remain in the magnitude of the core contraction (-0.1×10^{16} m^3/century with IQ range between -0.5 and 0.0×10^{16} m^3/century for OMZ_{20}) and the spatial redistribution of the hypoxic waters that fall in the transition regime between contraction and expansion. The model case studies presented here and in prior work provide insight on the source of uncertainties in the core and hypoxic range. The comparison of the two CanESM5 ESMs (with identical physical model) reveals that the ESM with the more complex biogeochemical module (CanESM5-CanOE) projects a smaller contraction of the core compared to its simpler biogeochemical counterpart (CanESM5). This suggests that changes in biological oxygen demand (which would act alongside mixing in contracting the core) are smaller in CanESM5-CanOE, or that negative feedbacks—acting against the contraction of the core—are at play. Additional biogeochemical processes represented in the more complex ESM could offset the oxygenation of the core (whether it is controlled by mixing changes or by changes in oxygen demand due to respiration) and thus stabilize the core volume. For instance, denitrification (switch to nitrate-based respiration at low oxygen levels, Swart et al., 2019a) and iron limitation which are represented in CanESM CanOE could buffer upper ocean productivity and O_2 changes in the OMZ core (e.g., Lachkar et al., 2016). Another example is the reduction of remineralization rates at low O_2, which could lead to shallower remineralization and more nutrient retention in response to the contraction of the core, potentially buffering the decline in export production and oxygen demand (Weber & Bianchi, 2020). In addition, prior work using two identical ESMs (identical biogeochemical and physical modules) but with different horizontal resolution in the ocean showed that a more realistic representation of the subtropical cells, and in particular the Equatorial current system, improved the representation of Pacific hypoxic waters but also minimized changes in their ventilation and volume (Busecke et al., 2019). Together, these

results suggest that more complex and realistic biogeochemical and ocean models improve the representation of the OMZ structure and stabilize its response to climate variability. This also suggests that the core contraction and OMZ expansion might lie in the lower bound of current ESM projections.

We show that changes in volume translate into changes in the depth of the upper OMZ boundary which shoals in the open ocean and along the Equator, and deepens in the eastern Pacific near-coastal regions where the core is projected to contract. Anticipating the influence of these changes on nitrous oxide production is not straightforward. The slight contraction and weak deepening of the OMZ core combined with the reduction in export production might reduce the production and release of nitrous oxide in the eastern Pacific (by limiting the supply of organic matter that can be remineralized at depth and shifting the nitrous oxide production site deeper in the water column, e.g., Ji et al., 2015; Landolfi et al., 2017; Martinez-Rey et al., 2015; Yang et al., 2017). In addition, one could expect that the relatively stable volume of hypoxic waters would yield minor changes in nitrous oxide production in anaerobic particulate niches (Bianchi et al., 2018). Yet, understanding the net effect on nitrous oxide emission to the atmosphere requires accounting for the spatial redistribution of the suboxic and hypoxic waters: how this impacts nitrous oxide production rates, but also how these changes in production influence the release of nitrous oxide to the atmosphere (via ocean advection and mixing). For instance, the effect of shallower hypoxic waters in the northern tropical Pacific Ocean could exceed the effect of deeper hypoxic waters in the eastern Pacific Ocean on the production and release of nitrous oxide. Process studies that include both a realistic description of the nitrogen cycling and ocean circulation in the Pacific OMZ are needed to assess the impact of suboxic and hypoxic waters redistribution on nitrous oxide emissions and climate. In contrast, the strong expansion and shoaling of low oxygenated waters expected in response to high greenhouse gas emissions will likely have strong detrimental ecological and economic consequences for ecosystem services such as fisheries by compressing the volume of oxygenated habitats available for macrofauna and increasing fishing pressure for species with high commercial value such as sardines, billfishes and tuna (Bertrand et al., 2011; Deutsch et al., 2020; Prince et al., 2010; Stramma et al., 2011).

Acronyms

OMZ	Oxygen Minimum Zone
ESM	Earth System Model

Acknowledgments
This study has been supported by the Cooperative Institute for Modeling the Earth System between NOAA GFDL and Princeton University, the High Meadows Environmental Institute CMI, the Sloan Foundation, and L.R. NSF CAREER Award Number 2042672 and the Gordon and Betty Moore Foundation (Grant 8434). The authors acknowledge the World Climate Research Programme, which, through its Working Group on Coupled Modelling, coordinated and promoted CMIP6. The authors thank the climate modeling groups for producing and making available their model output, the Earth System Grid Federation (ESGF) for archiving the data and providing access, and the multiple funding agencies who support CMIP6 and ESGF. The authors thank the pangeo project (R. P. Abernathey et al., 2021) and their cloud computing/storage resources, which were used for prototyping and software development. The authors further thank David Luet for his technical support and his help in creating a mirrored subset of the CMIP6 archive on the Princeton HPC, which was used for the final analysis. The authors thank John P. Dunne and three anonymous reviewers for their thorough review and insightful feedback.

Conflict of Interest

The authors declare no conflicts of interest relevant to this study.

Data Availability Statement

The code to reproduce our results is provided in a zenodo archive (https://zenodo.org/record/6803919). Processed data files, used to create plots are available in another zenodo archive (https://zenodo.org/record/6799335). Figures for the manuscript were created with xarray (Hoyer & Joseph, 2017), cartopy (Met Office, 2010–2015), cmocean (Thyng et al., 2016), xarrayutils (Busecke & Hogikyan, 2022), and matplotlib (Hunter, 2007). The authors additionally used NumPy (Harris et al., 2020), dask (Dask Development Team, 2016), pandas (pandas development team, 2020), cf-xarray (Cherian et al., 2022), rechunker (https://github.com/pangeo-data/rechunker), nc-time-axis (Little et al., 2022), and xgcm (R. Abernathey et al., 2020) for various processing task.

References

Abernathey, R., Busecke, J. J. M., Smith, T., Bot, S., Banihirwe, A., Zhang, C., et al. (2020). *xgcm/xgcm: v0.5.1*. Zenodo. https://doi.org/10.5281/zenodo.4097223

Abernathey, R., Squire, D., Nicholas, T., Bourbeau, J., Joseph, G., Spring, A., et al. (2021). xhistogram. https://doi.org/10.5281/zenodo.5757149

Abernathey, R. P., Augspurger, T., Banihirwe, A., Blackmon-Luca, C. C., Crone, T. J., Gentemann, C. L., et al. (2021). Cloud-native repositories for big scientific data. *Computing in Science & Engineering*, *23*(2), 26–35. https://doi.org/10.1109/mcse.2021.3059437

Babbin, A. R., Bianchi, D., Jayakumar, A., & Ward, B. B. (2015). Rapid nitrous oxide cycling in the suboxic ocean. *Science*, *348*(6239), 1127–1129. https://doi.org/10.1126/science.aaa8380

Bahl, A., Gnanadesikan, A., & Pradal, M.-A. (2019). Variations in ocean deoxygenation across Earth system models: Isolating the role of parameterized lateral mixing. *Global Biogeochemical Cycles*, *33*(6), 703–724. https://doi.org/10.1029/2018gb006121

Banihirwe, A., Long, M., bonnland, Kent, J., Spring, A., Busecke, J., et al. (2020). *intake/intake-esm: Intake-esm v2020.11.4*. Zenodo. https://doi.org/10.5281/zenodo.4243421

Bao, Y., & Li, Y. (2016). Simulations of dissolved oxygen concentration in CMIP5 Earth system models. *Acta Oceanologica Sinica*, *35*(12), 28–37. https://doi.org/10.1007/s13131-016-0959-x

Bentsen, M., Oliviè, D. J. L., Seland, Y., Toniazzo, T., Gjermundsen, A., Graff, L. S., et al. (2019a). *NCC NorESM2-mm model output prepared for CMIP6 CMIP*. Earth System Grid Federation. https://doi.org/10.22033/ESGF/CMIP6.506

Bentsen, M., Oliviè, D. J. L., Seland, Y., Toniazzo, T., Gjermundsen, A., Graff, L. S., et al. (2019b). *NCC NorESM2-mm model output prepared for CMIP6 ScenarioMIP*. Earth System Grid Federation. https://doi.org/10.22033/ESGF/CMIP6.608

Bertrand, A., Chaigneau, A., Peraltilla, S., Ledesma, J., Graco, M., Monetti, F., & Chavez, F. (2011). Oxygen: A fundamental property regulating pelagic ecosystem structure in the coastal southeastern tropical Pacific. *PLoS One*, *6*(12), e29558. https://doi.org/10.1371/journal.pone.0029558

Bianchi, D., Dunne, J. P., Sarmiento, J. L., & Galbraith, E. D. (2012). Data-based estimates of suboxia, denitrification, and N_2O production in the ocean and their sensitivities to dissolved O_2. *Global Biogeochemical Cycles*, *26*(2), GB2009. https://doi.org/10.1029/2011gb004209

Bianchi, D., Weber, T. S., Kiko, R., & Deutsch, C. (2018). Global niche of marine anaerobic metabolisms expanded by particle microenvironments. *Nature Geoscience*, *11*(4), 263–268. https://doi.org/10.1038/s41561-018-0081-0

Bopp, L., Le Quéré, C., Heimann, M., Manning, A. C., & Monfray, P. (2002). Climate-induced oceanic oxygen fluxes: Implications for the contemporary carbon budget. *Global Biogeochemical Cycles*, *16*(2), 6-1. https://doi.org/10.1029/2001gb001445

Bopp, L., Resplandy, L., Orr, J. C., Doney, S. C., Dunne, J. P., Gehlen, M., et al. (2013). Multiple stressors of ocean ecosystems in the 21st century: Projections with CMIP5 models. *Biogeosciences*, *21*(10), 6225–6245. https://doi.org/10.5194/bg-10-6225-2013

Bopp, L., Resplandy, L., Untersee, A., Le Mezo, P., & Kageyama, M. (2017). Ocean (de)oxygenation from the last glacial maximum to the twenty-first century: Insights from Earth system models. *Philosophical Transactions of the Royal Society A: Mathematical, Physical & Engineering Sciences*, *375*(2102), 20160323. https://doi.org/10.1098/rsta.2016.0323

Boucher, O., Denvil, S., Levavasseur, G., Cozic, A., Caubel, A., Foujols, M.-A., et al. (2018). *IPSL IPSL-CM6A-LR model output prepared for CMIP6 CMIP*. Earth System Grid Federation. https://doi.org/10.22033/ESGF/CMIP6.1534

Boucher, O., Denvil, S., Levavasseur, G., Cozic, A., Caubel, A., Foujols, M.-A., et al. (2019). *IPSL IPSL-CM6A-LR model output prepared for CMIP6 ScenarioMIP*. Earth System Grid Federation. https://doi.org/10.22033/ESGF/CMIP6.1532

Buchanan, P., & Tagliabue, A. (2021). The regional importance of oxygen demand and supply for historical ocean oxygen trends. *Geophysical Research Letters*, *48*(20), e2021GL094797. https://doi.org/10.1029/2021GL094797

Busecke, J., & Hogikyan (2022). *jbusecke/xarrayutils: v1.1.1*. Zenodo. https://doi.org/10.5281/zenodo.6360900

Busecke, J., Spring, A., Ritschel, M., Maroon, E., Nicholas, T., & readthedocs-assistant. (2022). jbusecke/xMIP: v0.6.1rc0 (v0.6.1rc0). Zenodo. https://doi.org/10.5281/zenodo.6812409

Busecke, J. J. M., Resplandy, L., & Dunne, J. P. (2019). The equatorial undercurrent and the oxygen minimum zone in the Pacific. *Geophysical Research Letters*, *46*(12), 6716–6725. https://doi.org/10.1029/2019gl082692

Cabré, A., Marinov, I., Bernardello, R., & Bianchi, D. (2015). Oxygen minimum zones in the tropical Pacific across CMIP5 models: Mean state differences and climate change trends. *Biogeosciences*, *12*(18), 5429–5454. https://doi.org/10.5194/bg-12-5429-2015

Cardich, J., Sifeddine, A., Salvatteci, R., Romero, D., Briceño-Zuluaga, F., Graco, M., et al. (2019). Multidecadal changes in marine subsurface oxygenation off Central Peru during the last ca. 170 years. *Frontiers in Marine Science*, *6*, 270. https://doi.org/10.3389/fmars.2019.00270

Chavez, F. P., Bertrand, A., Guevara-Carrasco, R., Soler, P., & Csirke, J. (2008). The northern Humboldt Current System: Brief history, present status and a view towards the future. *Progress in Oceanography*, *79*(2–4), 95–105. https://doi.org/10.1016/j.pocean.2008.10.012

Cherian, D., Almansi, M., Bourgault, P., Kent, J., Magin, J., & Thyng, K. (2022). *xarray-contrib/cf-xarray: v0.7.0*. Zenodo. https://doi.org/10.5281/zenodo.5899430

Christian, J. R., Denman, K. L., Hayashida, H., Holdsworth, A. M., Lee, W. G., Riche, O. G. J., et al. (2022). Ocean biogeochemistry in the Canadian Earth system model version 5.0.3: CanESM5 and CanESM5-CanOE. *Geoscientific Model Development*, *15*(11), 4393–4424. https://doi.org/10.5194/gmd-15-4393-2022

Cocco, V., Joos, F., Steinacher, M., Frölicher, T., Bopp, L., Dunne, J., et al. (2012). Oxygen and indicators of stress for marine life in multi-model global warming projections. *Biogeosciences Discussions*, *9*(8), 1849–1868. https://doi.org/10.5194/bg-10-1849-2013

Couespel, D., Lévy, M., & Bopp, L. (2019). Major contribution of reduced upper ocean oxygen mixing to global ocean deoxygenation in an Earth system model. *Geophysical Research Letters*, *46*(21), 12239–12249. https://doi.org/10.1029/2019gl084162

Czeschel, R., Stramma, L., Schwarzkopf, F. U., Giese, B. S., Funk, A., & Karstensen, J. (2010). Middepth circulation of the eastern tropical south Pacific and its link to the oxygen minimum zone. *Journal of Geophysical Research*, *116*(C1), C01015. https://doi.org/10.1029/2010jc006565

Dask Development Team. (2016). Dask: Library for dynamic task scheduling [Computer software manual]. Retrieved from https://dask.org

Deutsch, C., Berelson, W., Thunell, R., Weber, T., Tems, C., McManus, J., et al. (2014). Centennial changes in north Pacific anoxia linked to tropical trade winds. *Science*, *345*(6197), 665–668. https://doi.org/10.1126/science.1252332

Deutsch, C., Penn, J. L., & Seibel, B. (2020). Metabolic trait diversity shapes marine biogeography. *Nature*, *585*(7826), 557–562. https://doi.org/10.1038/s41586-020-2721-y

Doney, S. C., & Karnauskas, K. B. (2014). Oxygen and climate dynamics. *Nature Climate Change*, *4*(10), 862–863. https://doi.org/10.1038/nclimate2386

do Rosário Gomes, H., Goes, J., Matondkar, S., Buskey, E., Basu, S., Parab, S., & Thoppil, P. (2014). Massive outbreaks of *Noctiluca scintillans* blooms in the Arabian Sea due to spread of hypoxia. *Nature Communications*, *5*(1), 4862. https://doi.org/10.1038/ncomms5862

Duteil, O., Böning, C. W., & Oschlies, A. (2014). Variability in subtropical-tropical cells drives oxygen levels in the tropical Pacific Ocean. *Geophysical Research Letters*, *41*(24), 8926–8934. https://doi.org/10.1002/2014gl061774

Duteil, O., Frenger, I., & Getzlaff, J. (2021). The riddle of eastern tropical Pacific Ocean oxygen levels: The role of the supply by intermediate-depth waters. *Ocean Science*, *17*(5), 1489–1507. https://doi.org/10.5194/os-17-1489-2021

Duteil, O., Oschlies, A., & Böning, C. W. (2018). Pacific decadal oscillation and recent oxygen decline in the eastern tropical Pacific Ocean. *Biogeosciences Discussions*, *15*(23), 1–30. https://doi.org/10.5194/bg-15-7111-2018

Espinoza-Morriberón, D., Echevin, V., Gutiérrez, D., Tam, J., Graco, M., Ledesma, J., & Colas, F. (2021). Evidences and drivers of ocean deoxygenation off Peru over recent past decades. *Scientific Reports*, *11*(1), 20292. https://doi.org/10.1038/s41598-021-99876-8

Eyring, V., Bony, S., Meehl, G. A., Senior, C. A., Stevens, B., Stouffer, R. J., & Taylor, K. E. (2016). Overview of the Coupled Model Intercomparison Project Phase 6 (CMIP6) experimental design and organization. *Geoscientific Model Development*, *9*(5), 1937–1958. https://doi.org/10.5194/gmd-9-1937-2016

Firing, E., FilipeBarna, A., & Abernathey, R. (2021). TEOS-10/GSW-Python: v3.4.1.post0. https://doi.org/10.5281/zenodo.5214122

Frölicher, T. L., Aschwanden, M. T., Gruber, N., Jaccard, S., Dunne, J. P., & Paynter, D. (2020). Contrasting upper and deep ocean oxygen response to protracted global warming. *Global Biogeochemical Cycles*, *34*(8), e2020GB006601. https://doi.org/10.1029/2020gb006601

Garcia, H. E., Locarnini, R. A., Boyer, T. P., & Antonov, J. I. (2006). World Ocean Atlas 2005, vol. 3, dissolved oxygen, apparent oxygen utilization, and oxygen saturation.

Gnanadesikan, A., Dunne, J., & John, J. (2012). Understanding why the volume of suboxic waters does not increase over centuries of global warming in an Earth system model. *Biogeosciences*, *9*(3), 1159–1172. https://doi.org/10.5194/bg-9-1159-2012

Gnanadesikan, A., Russell, J. L., & Fanrong, Z. (2007). How does ocean ventilation change under global warming. *Ocean Science*, *3*(1), 43–53. https://doi.org/10.5194/os-3-43-2007

Good, P., Sellar, A., Tang, Y., Rumbold, S., Ellis, R., Kelley, D., et al. (2019). *MOHC UKESM1.0-LL model output prepared for CMIP6 ScenarioMIP*. Earth System Grid Federation. https://doi.org/10.22033/ESGF/CMIP6.1567

Guo, H., John, J. G., Blanton, C., McHugh, C., Nikonov, S., Radhakrishnan, A., et al. (2018a). *NOAA-GFDL GFDL-CM4 model output*. Earth System Grid Federation. https://doi.org/10.22033/ESGF/CMIP6.1402

Guo, H., John, J. G., Blanton, C., McHugh, C., Nikonov, S., Radhakrishnan, A., et al. (2018b). *NOAA-GFDL GFDL-CM4 model output prepared for CMIP6 ScenarioMIP*. Earth System Grid Federation. https://doi.org/10.22033/ESGF/CMIP6.9242

Hajima, T., Abe, M., Arakawa, O., Suzuki, T., Komuro, Y., Ogura, T., et al. (2019). *MIROC MIROC-ES2L model output prepared for CMIP6 CMIP*. Earth System Grid Federation. https://doi.org/10.22033/ESGF/CMIP6.902

Harper, S. (2000). Thermocline ventilation and pathways of tropical–subtropical water mass exchange. *Tellus A: Dynamic Meteorology and Oceanography*, *52*(3), 330–345. https://doi.org/10.3402/tellusa.v52i3.12269

Harris, C. R., Millman, K. J., Van Der Walt, S. J., Gommers, R., Virtanen, P., Cournapeau, D., et al. (2020). Array programming with NumPy. *Nature*, *585*(7825), 357–362. https://doi.org/10.1038/s41586-020-2649-2

Hoyer, S., & Joseph, H. (2017). xarray: N-D labeled arrays and datasets in Python. *Journal of Open Research Software*, *5*(1), 10. https://doi.org/10.5334/jors.148

Hunter, J. D. (2007). Matplotlib: A 2D graphics environment. *Computing in Science & Engineering*, *9*(3), 90–95. https://doi.org/10.1109/MCSE.2007.55

Ito, T., Minobe, S., Long, M. C., & Deutsch, C. (2017). Upper ocean O_2 trends: 1958–2015. *Geophysical Research Letters*, *44*(9), 4214–4223. https://doi.org/10.1002/2017gl073613

Ji, Q., Babbin, A. R., Jayakumar, A., Oleynik, S., & Ward, B. B. (2015). Nitrous oxide production by nitrification and denitrification in the eastern tropical south Pacific oxygen minimum zone. *Geophysical Research Letters*, *42*(24), 10755–10764. https://doi.org/10.1002/2015gl066853

John, J. G., Blanton, C., McHugh, C., Radhakrishnan, A., Rand, K., Vahlenkamp, H., et al. (2018). *NOAA-GFDL GFDL-ESM4 model output prepared for CMIP6 ScenarioMIP*. Earth System Grid Federation. https://doi.org/10.22033/ESGF/CMIP6.1414

Jungclaus, J., Bittner, M., Wieners, K.-H., Wachsmann, F., Schupfner, M., Legutke, S., et al. (2019). *MPI-M MPIESM1.2-Hr model output prepared for CMIP6 CMIP*. Earth System Grid Federation. https://doi.org/10.22033/ESGF/CMIP6.741

Karnauskas, K. B., Jakoboski, J., Johnston, T. M. S., Owens, W. B., Rudnick, D. L., & Todd, R. E. (2020). The Pacific equatorial undercurrent in three generations of global climate models and glider observations. *Journal of Geophysical Research: Oceans*, *125*(11), e2020JC016609. https://doi.org/10.1029/2020jc016609

Keeling, R. F., Körtzinger, A., & Gruber, N. (2010). Ocean deoxygenation in a warming world. *Annual Review of Marine Science*, *2*(1), 199–229. https://doi.org/10.1146/annurev.marine.010908.163855

Krasting, J. P., John, J. G., Blanton, C., McHugh, C., Nikonov, S., Radhakrishnan, A., et al. (2018). *NOAA-GFDL GFDL-ESM4 model output prepared for CMIP6 CMIP*. Earth System Grid Federation. https://doi.org/10.22033/ESGF/CMIP6.1407

Kwiatkowski, L., Torres, O., Bopp, L., Aumont, O., Chamberlain, M., Christian, J., et al. (2020). Twenty-first century ocean warming, acidification, deoxygenation, and upper ocean nutrient decline from CMIP6 model projections. *Biogeosciences*, *17*(13), 3439–3470. https://doi.org/10.5194/bg-17-3439-2020

Lachkar, Z., Smith, S., Lévy, M., & Pauluis, O. (2016). Eddies reduce denitrification and compress habitats in the Arabian Sea. *Geophysical Research Letters*, *43*(17), 9148–9156. https://doi.org/10.1002/2016gl069876

Landolfi, A., Somes, C. J., Koeve, W., Zamora, L. M., & Oschlies, A. (2017). Oceanic nitrogen cycling and N_2O flux perturbations in the anthropocene. *Global Biogeochemical Cycles*, *31*(8), 1236–1255. https://doi.org/10.1002/2017gb005633

Levin, L. A. (2018). Manifestation, drivers, and emergence of open ocean deoxygenation. *Annual Review of Marine Science*, *10*(1), 229–260. https://doi.org/10.1146/annurev-marine-121916-063359

Lévy, M., Resplandy, L., Palter, J., Couespel, D., & Lachkar, Z. (2021). The crucial contribution of mixing to present and future ocean oxygen distribution. Retrieved from https://hal.archives-ouvertes.fr/

Little, B., lbdreyer, Clark, S., Filipe, Busecke, J., Elson, P., et al. (2022). *SciTools/nc-time-axis: v1.4.1*. Zenodo. https://doi.org/10.5281/zenodo.6472641

Llanillo, P. J., Pelegrí, J. L., Talley, L. D., Peña-Izquierdo, J., & Cordero, R. R. (2018). Oxygen pathways and budget for the eastern south Pacific oxygen minimum zone. *Journal of Geophysical Research: Oceans*, *123*(3), 1722–1744. https://doi.org/10.1002/2017jc013509

Luyten, J., Pedlosky, J., & Stommel, H. (1983). The ventilated thermocline. *Journal of Physical Oceanography*, *13*(2), 292–309. https://doi.org/10.1175/1520-0485(1983)013<0292:tvt>2.0.co;2

Margolskee, A., Frenzel, H., Emerson, S., & Deutsch, C. (2019). Ventilation pathways for the north Pacific oxygen deficient zone. *Global Biogeochemical Cycles*, *33*(7), 875–890. https://doi.org/10.1029/2018GB006149

Martinez-Rey, J., Bopp, L., Gehlen, M., Tagliabue, A., & Gruber, N. (2015). Projections of oceanic N_2O emissions in the 21st century using the IPSL Earth system model. *Biogeosciences*, *12*(13), 4133–4148. https://doi.org/10.5194/bg-12-4133-2015

Met Office. (2010–2015). Cartopy: A cartographic python library with a matplotlib interface [Computer software manual]. Retrieved from http://scitools.org.uk/cartopy

Miller, D., Poucher, S., & Coiro, L. (2002). Determination of lethal dissolved oxygen levels for selected marine and estuarine fishes, crustaceans, and a bivalve. *Marine Biology*, *140*(2), 287–296. https://doi.org/10.1007/s002270100702

O'Neill, B. C., Tebaldi, C., van Vuuren, D. P., Eyring, V., Friedlingstein, P., Hurtt, G., et al. (2016). The scenario model intercomparison project (ScenarioMIP) for CMIP6. *Geoscientific Model Development*, *9*(9), 3461–3482. https://doi.org/10.5194/gmd-9-3461-2016

Palter, J. B., & Trossman, D. S. (2018). The sensitivity of future ocean oxygen to changes in ocean circulation. *Global Biogeochemical Cycles*, *32*(5), 738–751. https://doi.org/10.1002/2017gb005777

Pandas Development Team, T. (2020). *pandas-dev/pandas: Pandas*. Zenodo. https://doi.org/10.5281/zenodo.3509134

Paulmier, A., & Ruiz-Pino, D. (2009). Oxygen minimum zones (OMZs) in the modern ocean. *Progress in Oceanography*, *80*(3), 113–128. https://doi.org/10.1016/j.pocean.2008.08.001

Pedlosky, J. (1986). The buoyancy and wind-driven ventilated thermocline. *Journal of Physical Oceanography*, *16*(6), 1077–1087. https://doi.org/10.1175/1520-0485(1986)016<1077:tbawdv>2.0.co;2

Petrie, R., Denvil, S., Ames, S., Levavasseur, G., Fiore, S., Allen, C., et al. (2021). Coordinating an operational data distribution network for CMIP6 data. *Geoscientific Model Development*, *14*(1), 629–644. https://doi.org/10.5194/gmd-14-629-2021

Prince, E. D., Luo, J., Phillip Goodyear, C., Hoolihan, J. P., Snodgrass, D., Orbesen, E. S., et al. (2010). Ocean scale hypoxia-based habitat compression of Atlantic istiophorid billfishes. *Fisheries Oceanography*, *19*(6), 448–462. https://doi.org/10.1111/j.1365-2419.2010.00556.x

Resplandy, L. (2018). Will ocean zones with low oxygen levels expand or shrink. *Nature*, *557*(7705), 314–315. https://doi.org/10.1038/d41586-018-05034-y

Schmidtko, S., Stramma, L., & Visbeck, M. (2017). Decline in global oceanic oxygen content during the past five decades. *Nature*, *542*(7641), 335–339. https://doi.org/10.1038/nature21399

Schott, F. A., McCreary, J. P., Jr., & Johnson, G. C. (2004). Shallow overturning circulations of the tropical-subtropical oceans. *Washington DC American Geophysical Union Geophysical Monograph Series*, *147*, 261–304.

Schupfner, M., Wieners, K.-H., Wachsmann, F., Steger, C., Bittner, M., Jungclaus, J., et al. (2019). *DKRZ MPI-ESM1.2-HR model output prepared for CMIP6 ScenarioMIP*. Earth System Grid Federation. https://doi.org/10.22033/ESGF/CMIP6.2450

Seferian, R. (2018). *CNRM-CERFACS CNRM-ESM2-1 model output prepared for CMIP6 CMIP*. Earth System Grid Federation. https://doi.org/10.22033/ESGF/CMIP6.1391

Seferian, R. (2019). *CNRM-CERFACS CNRM-ESM2-1 model output prepared for CMIP6 ScenarioMIP*. Earth System Grid Federation. https://doi.org/10.22033/ESGF/CMIP6.1395

Séférian, R., Berthet, S., Yool, A., Palmiéri, J., Bopp, L., Tagliabue, A., et al. (2020). Tracking improvement in simulated marine biogeochemistry between CMIP5 and CMIP6. *Current Climate Change Reports*, *6*(3), 1–25. https://doi.org/10.1007/s40641-020-00160-0

Seland, Y., Bentsen, M., Oliviè, D. J. L., Toniazzo, T., Gjermundsen, A., Graff, L. S., et al. (2019a). *NCC NORESM2-LM model output prepared for CMIP6 CMIP*. Earth System Grid Federation. https://doi.org/10.22033/ESGF/CMIP6.502

Seland, Y., Bentsen, M., Oliviè, D. J. L., Toniazzo, T., Gjermundsen, A., Graff, L. S., et al. (2019b). *NCC NORESM2-LM model output prepared for CMIP6 ScenarioMIP*. Earth System Grid Federation. https://doi.org/10.22033/ESGF/CMIP6.604

Shigemitsu, M., Yamamoto, A., Oka, A., & Yamanaka, Y. (2017). One possible uncertainty in CMIP5 projections of low oxygen water volume in the eastern tropical Pacific. *Global Biogeochemical Cycles*, *31*(5), 804–820. https://doi.org/10.1002/2016gb005447

Stramma, L., Johnson, G. C., Firing, E., & Schmidtko, S. (2010). Eastern Pacific oxygen minimum zones: Supply paths and multidecadal changes. *Journal of Geophysical Research*, *115*(C9), C09011. https://doi.org/10.1029/2009jc005976

Stramma, L., Johnson, G. C., Sprintall, J., & Mohrholz, V. (2008). Expanding oxygen-minimum zones in the tropical oceans. *Science*, *320*(5876), 655–658. https://doi.org/10.1126/science.1153847

Stramma, L., Prince, E. D., Schmidtko, S., Luo, J., Hoolihan, J. P., Visbeck, M., et al. (2011). Expansion of oxygen minimum zones may reduce available habitat for tropical pelagic fishes. *Nature Climate Change*, *2*(1), 33–37. https://doi.org/10.1038/nclimate1304

Swart, N. C., Cole, J. N., Kharin, V. V., Lazare, M., Scinocca, J. F., Gillett, N. P., et al. (2019b). *CCCma CanESM5-CanOE model output prepared for CMIP6 CMIP*. Earth System Grid Federation. https://doi.org/10.22033/ESGF/CMIP6.10205

Swart, N. C., Cole, J. N., Kharin, V. V., Lazare, M., Scinocca, J. F., Gillett, N. P., et al. (2019c). *CCCma CanESM5-CanOE model output prepared for CMIP6 ScenarioMIP*. Earth System Grid Federation. https://doi.org/10.22033/ESGF/CMIP6.10207

Swart, N. C., Cole, J. N., Kharin, V. V., Lazare, M., Scinocca, J. F., Gillett, N. P., et al. (2019d). *CCCma CanESM5 model output prepared for CMIP6 CMIP*. Earth System Grid Federation. https://doi.org/10.22033/ESGF/CMIP6.1303

Swart, N. C., Cole, J. N., Kharin, V. V., Lazare, M., Scinocca, J. F., Gillett, N. P., et al. (2019e). *CCCma CanESM5 model output prepared for CMIP6 ScenarioMIP*. Earth System Grid Federation. https://doi.org/10.22033/ESGF/CMIP6.1317

Swart, N. C., Cole, J. N. S., Kharin, V. V., Lazare, M., Scinocca, J. F., Gillett, N. P., et al. (2019a). The Canadian Earth system model version 5 (CanESM5.0.3). *Geoscientific Model Development*, *12*(11), 4823–4873. https://doi.org/10.5194/gmd-12-4823-2019

Tachiiri, K., Abe, M., Hajima, T., Arakawa, O., Suzuki, T., Komuro, Y., et al. (2019). *MIROC MIROC-ES2L model output prepared for CMIP6 ScenarioMIP*. Earth System Grid Federation. https://doi.org/10.22033/ESGF/CMIP6.936

Tang, Y., Rumbold, S., Ellis, R., Kelley, D., Mulcahy, J., Sellar, A., et al. (2019). *MOHC UKESM1.0-LL model output prepared for CMIP6 CMIP*. Earth System Grid Federation. https://doi.org/10.22033/ESGF/CMIP6.1569

Taylor, K. E., Stouffer, R. J., & Meehl, G. A. (2011). An overview of CMIP5 and the experiment design. *Bulletin of the American Meteorological Society Bull. Amer. Meteor. Soc.*, *93*(4), 485–498. https://doi.org/10.1175/bams-d-11-00094.1

Thyng, K. M., Greene, C. A., Hetland, R. D., Zimmerle, H. M., & DiMarco, S. F. (2016). True colors of oceanography: Guidelines for effective and accurate colormap selection. *Oceanography*, *29*(3), 9–13. https://doi.org/10.5670/oceanog.2016.66

Vaquer-Sunyer, R., & Duarte, C. M. (2008). Thresholds of hypoxia for marine biodiversity. *Proceedings of the National Academy of Sciences*, *105*(40), 15452–15457. https://doi.org/10.1073/pnas.0803833105

Weber, T., & Bianchi, D. (2020). Efficient particle transfer to depth in oxygen minimum zones of the Pacific and Indian Oceans. *Frontiers of Earth Science*, *8*, 376. https://doi.org/10.3389/feart.2020.00376

Wieners, K.-H., Giorgetta, M., Jungclaus, J., Reick, C., Esch, M., Bittner, M., et al. (2019a). *MPI-M MPIESM1.2-LR model output prepared for CMIP6 CMIP*. Earth System Grid Federation. https://doi.org/10.22033/ESGF/CMIP6.742

Wieners, K.-H., Giorgetta, M., Jungclaus, J., Reick, C., Esch, M., Bittner, M., et al. (2019b). *MPI-M MPIESM1.2-LR model output prepared for CMIP6 ScenarioMIP*. Earth System Grid Federation. https://doi.org/10.22033/ESGF/CMIP6.793

Yang, S., Gruber, N., Long, M. C., & Vogt, M. (2017). Enso-driven variability of denitrification and suboxia in the eastern tropical Pacific Ocean. *Global Biogeochemical Cycles*, *31*(10), 1470–1487. https://doi.org/10.1002/2016gb005596

Yukimoto, S., Koshiro, T., Kawai, H., Oshima, N., Yoshida, K., Urakawa, S., et al. (2019a). *MRI MRI-ESM2.0 model output prepared for CMIP6 CMIP*. Earth System Grid Federation. https://doi.org/10.22033/ESGF/CMIP6.621

Yukimoto, S., Koshiro, T., Kawai, H., Oshima, N., Yoshida, K., Urakawa, S., et al. (2019b). *MRI MRI-ESM2.0 model output prepared for CMIP6 ScenarioMIP*. Earth System Grid Federation. https://doi.org/10.22033/ESGF/CMIP6.638

Zhuang, J., Dussin, R., Huard, D., Bourgault, P., Banihirwe, A., Hamman, J., et al. (2021). *pangeo-data/xESMF: v0.5.2*. Zenodo. https://doi.org/10.5281/zenodo.4464833

Ziehn, T., Chamberlain, M., Lenton, A., Law, R., Bodman, R., Dix, M., et al. (2019a). *CSIRO ACCESS-ESM1.5 model output prepared for CMIP6 CMIP*. Earth System Grid Federation. https://doi.org/10.22033/ESGF/CMIP6.2288

Ziehn, T., Chamberlain, M., Lenton, A., Law, R., Bodman, R., Dix, M., et al. (2019b). *CSIRO ACCESS-ESM1.5 model output prepared for CMIP6 ScenarioMIP*. Earth System Grid Federation. https://doi.org/10.22033/ESGF/CMIP6.2291